Acidic property of YNU-5 zeolite influenced by its unique micropore system

Naonobu Katada, Kana Yamamoto, Moeri Fukui, Kai Asanuma, Satoshi Inagaki, Kazuki Nakajima, Satoshi Suganuma, Etsushi Tsuji, Ana Palcic, Valentin Valtchev, et al.

Acidic property of YNU-5 zeolite influenced by its unique micropore system

Naonobu Katada [a]*, Kana Yamamoto [a], Moeri Fukui [a], Kai Asanuma [b], Satoshi Inagaki [b], Kazuki Nakajima [a], Satoshi Suganuma [a], Etsushi Tsuji [a], Ana Palcic [c], Valentin Valtchev [d], Petko St. Petkov [e], Kristina Simeonova [e], Georgi N. Vayssilov [e], Yoshihiro Kubota [b]*

a Center for Research on Green Sustainable Chemistry, Tottori University, 4-101 Koyama-cho Minami, Tottori 680-8552, Japan

b Division of Materials Science and Chemical Engineering, Yokohama National University, 79-5 Tokiwadai, Hodogaya-ku, Yokohama 240-8501, Japan

c Ruđer Bošković Institute, Division of Materials Chemistry, Laboratory for Synthesis of New Materials, Bijenička cesta 54, Zagreb, Croatia

d Normandie Univ, ENSICAEN, UNICAEN, CNRS, Laboratoire Catalyse et Spectrochimie, 14050 Caen, France

e Faculty of Chemistry and Pharmacy, University of Sofia, blvd J. Baucher 1, 1126 Sofia, Bulgaria

Abstract

YNU-5 zeolite has the **YFI**-type framework with a 12-12-8-ring system (2-dimensional 12-oxygen membered ring pores 3-dimensionally connected by twin 8-ring channels), and isolated 8-ring channels separated from the system by a thin (mono-atomic silicate) wall. In this study, the acidic property of YNU-5 zeolite was analyzed mainly by means of the ammonia IRMS-TPD (infrared/mass spectroscopy temperature-programmed desorption) method. In addition, the accessibility of acid sites was evaluated through adsorption of pyridine. The number of Brønsted acid sites approximately agreed with the number of Al atoms, and the amount of Lewis acid sites was negligible, indicating that most acid sites have the nature of bridging Si(OH)Al group in the

YFI framework. Most of the Brønsted acidic OH groups on the YNU-5 zeolites (including the dealuminated samples) reacted with pyridine vapor at 343 K to form pyridinium cations, indicating that the Brønsted acid sites are highly accessible through the 12-12-8-ring system. Enthalpy of ammonia desorption from the Brønsted acid site, which can be an index of acid strength or reactivity of the acid site with a basic reactant, was in the following order: **FAU** < **MOR** (12-ring) ≈ ***BEA** < **MFI** < **MWW** ≈ **YFI** < **MOR** (8-ring), indicating the markedly large ammonia desorption enthalpy on the YNU-5 zeolite compared to the other 12-ring zeolites. The DFT calculations suggest that the Brønsted acidic protons with especially high ammonia desorption enthalpy are located in the isolated 8-ring but accessible from the 12-12-8-ring system side. In addition, dealumination at a high temperature under the reflux conditions with nitric acid resulted in the preferential removal of Brønsted acid sites with low ammonia desorption enthalpy, probably in the 12-12-8-ring system. The presence of reactive Brønsted acid sites in the isolated 8-ring, accessibility to them from the 12-12-8-ring system, and preferential removal of the Brønsted acid sites from the 12-12-8-ring system are reasonably consistent with the previously reported catalytic properties for dimethyl ether-to-olefin reaction.

Keywords

YNU-5 zeolite, YFI, Brønsted acid strength, ammonia IRMS-TPD, accessibility

Introduction

Zeolite is a family of materials with aluminosilicate composition and micropores ascribed to a 3-dimensional crystalline framework [1-6]. To date, there are more than 250 zeolite framework types, as a three-letter code is given to each framework type by the structure commission of the

International Zeolite Association [7]. The most widely used framework types are **MFI**, ***BEA**, **MWW**, **FAU**, **MOR**, **CHA** and **FER**. They are used as solid acid catalysts for various chemical and petroleum refinery processes due to their unique properties including strong acidity, high thermal stability, and shape-selectivity. These functions of zeolites have supported the mankind's culture throughout the petroleum era by realizing the efficient conversion of hydrocarbons into valued fuels and chemical products generating relatively low environmental pollution [8]. Nowadays, applications of zeolites are extended not only to catalysts for fossil hydrocarbons conversion [9], but also to environmentally benign organic synthesis and conversion of bio-derived compounds into useful chemicals [10], as well as non-catalytic usages of zeolites range from environmental protection and clean energy [11] to biomedical engineering [12], medical and biological fields [13].

The zeolites have ordered micropores, which are classified with respect to their opening size into small (8-ring), medium (10-ring), large (12-ring), and extra-large (>12-ring) ones. It is still challenging to synthesize an aluminosilicate zeolite, which shows high thermal and chemical stability, with extra-large pore windows. Therefore the maximum ring size of pore openings in aluminosilicate zeolites has practically been limited to 12-ring whose size is 0.6−0.7 nm [7]. The quest of large pore zeolites that are capable of converting heavy hydrocarbons is urgent, and hence the generation of strong Brønsted acid sites with high catalytic activity on the wall of 12-ring micropores is necessary.

However, strong and/or catalytically-active Brønsted acid sites tend to be situated in the smaller pores of zeolite. Several examples are listed below:

(1) The order of activity for Brønsted acid-catalyzed reactions over zeolites per one acid site is **FAU** [large cavity (supercage) connected by 12-ring windows, 1.3 nm] < ***BEA** [3-dimensional 12-ring channels, 0.6 nm] < **MFI** [10-ring, 0.54−0.57 nm] [14-17]. This allows multiple interpretations;

(1a) the strong Brønsted acid site is difficult to be formed on the wall of large pore; (1b) the high Si/Al ratio of **MFI** provides the high catalytic activity, and high silica, large-pore zeolite that is more active than **MFI** has not been found. In any cases of (1a) or (1b), catalytically-active Brønsted acid sites tend to be situated in the smaller zeolite pores.

(2) Infrared (IR) spectroscopy identifies the Brønsted acidic OH groups, i.e. [Si(OH)Al] moieties, in 8- and 12-rings of **MOR** [18-20]; only OH in 12-ring is accessible by pyridine [19-21], and OH in 8-ring has stronger Brønsted acidity than that in 12-ring [20, 22, 23].

(3) The ammonia desorption enthalpy (i.e., ammonia adsorption heat) is higher on the Brønsted acid in the smaller sodalite cage than that in the larger supercage in **FAU** type zeolite [24].

(4) In the field of mesoporous silica [25-27], it has still been difficult to find or construct strong or active Brønsted acid sites on mesoporous aluminosilicates [28]. These trends imply the difficulty of generating catalytically-active Brønsted acid sites accessible by large molecules.

The Brønsted acid site is generated by isomorphous substitution of tetravalent Si atom with trivalent Al atom (this means "replacement of Si by Al" in this manuscript) in the zeolite framework [29]. Therefore, the Brønsted acid site is a bridged Al−O−Si unit in which a proton is attached to the oxygen atom, i.e. [Al(OH)Si] moiety. The Brønsted acid site strength is dependent on factors such as framework type [15], Al concentration [30] and the presence of extra-framework Al species [31-33], even if the material is limited to pure aluminosilicate. Quantum chemistry analysis suggests that the features such as AlO distance and AlOSi angle influence the Brønsted acid strength [34], and it is considered that the framework topology influences on the Brønsted acid strength through such geometrical parameters. Katada et al. propose that the shorter AlO distance gives the higher ammonia desorption energy (one of the parameters showing Brønsted acid strength) owing to the nature of Al strongly electron-withdrawing from SiOH [35-37]. Because compression from both ends of the [Al(OH)Si] unit is necessary to shorten the AlO distance, it is

speculated that the wall of small pores with large curvature and high density of atoms provide the environment to generate the strong Brønsted acidity. In other words, it should be difficult to form a strong Brønsted acid site on a wall of large pore or on a plane. However, microstructure of zeolite has unlimited variation, and it should be possible to find unique structure with both of strong Brønsted acidity and high accessibility [38].

Recently, Kubota and co-workers synthesized a new type of zeolite material denoted as YNU-5 (Yokohama National University-5) [39]. The **YFI** framework consists of 12-12-8-ring system (2-dimensional 12-ring network 3-dimensionally connected by 8-ring windows) and individual straight 8-ring channels (hereafter "isolated 8-ring"). The large micropore system (12-12-8-ring system) is separated from the small micropore (isolated 8-ring) by a monoatomic silicate layer in the **YFI** framework (Figure 1).

The YNU-5 zeolite has high stability even after conversion into NH_4-form, subsequent calcination into H-form and during treatments in an acidic medium [39, 40], which brings it usefulness as a solid acid catalyst. In addition, dealumination of the YNU-5 zeolite for adjusting the concentration of acid sites is possible because of its high stability in the acidic medium [41]. Catalytic activity of the YNU-5 zeolite for typical Brønsted acid-catalyzed reactions such as dimethyl ether-to-olefin [42] and hexane cracking [43] have been reported.

The 8-rings in **YFI** framework are promising to have strong Brønsted acidity due to the geometrical nature. Among the 8-rings, the twin 8-ring is directly connected to the 2-dimensional 12-ring network and thus obviously expected to be accessible by a bulky molecule inside the 12-ring. In contrast, it seems that only very small molecules can enter into the isolated 8-ring. It is also reasonable to speculate that the aluminum atoms tend to remain in the hindered space inside isolated narrow channels even after almost all Al atoms are removed through deep dealumination by acid-treatment. Nevertheless, the highly dealuminated YNU-5 catalyst shows enough activity for

the reaction of the molecules too bulky to enter into 8-ring while less bulky than 12-ring size [42, 43]. Based on such an observation, it may be possible for the bulky molecule to access the acid site in the isolated 8-ring in some way. A closer look at the framework structure allows us to say that the isolated 8-ring is only separated from the 12-12-8-ring system by a mono-atomic silicate wall. The remaining framework Al inside isolated 8-ring channels are expected to afford strong Brønsted acidity according to the explanations given above. Therefore, the YNU-5 zeolite is expected to have strong Brønsted acid sites accessible from the 12-ring. On these backgrounds, this study focuses on the acidic property of YNU-5 zeolite.

Temperature-programmed desorption (TPD) method using vapor of basic probe adsorbate is suitable for accurate quantification of the number of adsorption sites, as well as for estimating such a kinetic parameter as activation energy for desorption or such a thermodynamic parameter as enthalpy of desorption (adsorption heat) [44]. Ammonia is most frequently used as the probe adsorbate because of the small molecular size is and the low reactivity for side reactions such as decomposition [45]. Disadvantages of the ammonia TPD caused by multiple types of ammonia adsorption and influences of re-adsorption [46] have been overcome as follows.

The adsorption of ammonia includes the chemisorption on both Brønsted and Lewis acid sites, as well as the physical adsorption, often on NH_4^+ cation which had been adsorbed on the Brønsted acid site [47-51]. Extraction of information on the acid sites or Brønsted acid sites needs help of infrared (IR) spectroscopy which can identify the NH_4^+ cation formed on Brønsted acid site, and the NH_3 species coordinated to Lewis acid site and sometimes physically adsorbed [52, 53].

On the other hand, it has been found that equilibrium exists during the TPD of ammonia over a wide range of solid acids, various zeolites [54] and non-zeolitic materials [23, 55, 56]. It simplifies the argument, because the possibility of diffusion control is ignored under the equilibrium conditions [44]. However, the equilibrium conditions make it impossible to obtain

kinetic parameters, because the apparent desorption rate is influenced by the re-adsorption [46, 57], and it looks a disadvantage. Nevertheless, a thermodynamic parameter such as molar standard enthalpy of ammonia desorption (= adsorption heat, hereafter ΔH) is calculated from the TPD profile based on theories assuming the equilibrium control [15, 44, 58]. This gives an advantage of the ammonia TPD, because one can calculate equilibrium constant and Hammett index at any temperature from ΔH [59], giving the strength of acid-base interaction according to the traditional definition of acid strength [60].

Therefore, combining the ammonia TPD and IR techniques makes it possible to determine the number and strength of each of Brønsted and Lewis acid sites on a solid, and we have developed an ammonia IRMS (infrared / mass spectroscopy)-TPD method [23, 61].

Even after the disadvantages (multiple types of adsorption and influence of re-adsorption) have been overcome, we have an argument on the interpretation of ΔH or ammonia desorption energy, because the quantum chemistry clarifies that the order the ammonia desorption energy on various zeolites disagrees with the order of deprotonation energy, which is considered to be an index of intrinsic Brønsted acid strength [62, 63]. The ΔH includes the energy of stabilization of NH_4^+ by the solid surface [17], and therefore, the feature of the stabilization strength is speculated to influence ΔH values on zeolites. Further details have been under discussion [63], but ΔH on Brønsted acid site should represent the strength of stabilization of a typical basic molecule by the Brønsted acid site, and, in a fact, strong relationships between activation energies of some acid-catalyzed reactions and ΔH have been observed [64, 65]. Therefore, ΔH has been widely used to exhibit the efficiency of Brønsted acid site on a solid acid for acid-catalyzed reactions.

For these reasons, we here applied the ammonia IRMS-TPD to measure the total acidic property of YNU-5 zeolite. Furthermore, the accessibility of a large molecule to the Brønsted acid site was investigated with an aid of pyridine adsorption [66]. In addition, IR spectroscopy of

adsorbed deuterated acetonitrile (CD_3CN, acetonitrile-d_3) [67] was also adopted to quantify the acid sites to support the above experiments. The set of experimental data provides deep insight into YNU-5's acidic properties and potential as a heterogeneous catalyst.

Dealumination of the YNU-5 zeolite has been achieved by acid treatment in an aqueous medium. It has been clarified that microstructure and physicochemical property of the dealuminated sample are considerably dependent on the temperature of acid treatment [41]. A treatment with nitric acid at 353 K yields a **YFI** type zeolite with considerable concentration of SiOH groups (most probably "site defects" which mean framework vacancies) due to dislodging of Al atoms from the framework. The thermal stability of the thus dealuminated sample was low; heating at 923 K drastically reduced the crystallinity. At a higher temperature (aqueous nitric acid solution was refluxed under atmospheric pressure in an oil bath which was kept at 403 K), the SiOH groups were diminished due to migration of Si atoms filling the defects. The extent of dealumination (resultant Si/Al ratio or [Al], i.e., Al concentration in the solid) can be adjusted by selecting the concentration of nitric acid. Thus, YNU-5 zeolites with high concentration of defects and low thermal stability (hereafter termed unstable deAl-YNU-5) and those with high thermal stability (stable deAl-YNU-5) possessing various [Al] can be prepared [41].

It has been known that moderate concentration of Brønsted acid sites is preferred to generate high catalytic activity of **MFI** and other medium pore zeolites for reactions of mono-cyclic aromatic hydrocarbons [68]. Therefore, investigation of the acidic properties of the dealuminated YNU-5 zeolites will be important for the use of solid acid catalysts. The properties of stabilized and unstabilized deAl-YNU-5 samples at the same level of the Si/Al ratio were also compared in this study.

Experimental and Computational Methods

Details of experimental and calculation methods are shown in Supporting Information.

YNU-5 zeolite was synthesized according to the previously reported method [39], and after calcination, ion-exchanged with NH_4NO_3 into NH_4-YNU-5. In the ammonia IRMS-TPD and pyridine / acetonirile-d_3 adsorption experiments, the basic probes were adsorbed after the conversion of the NH_4-form into H-form without exposure of the H-form sample to the ambient atmosphere; this procedure was adopted to avoid from unexpected dealumination of the YNU-5 zeolite with high aluminum concentration. It has been known that the H-form zeolite with high aluminum concentration (i.e., high H concentration) causes dealumination by contact with humid atmosphere even at the room temperature [69], affecting the acidic property through loss of a part of ion exchange sites and formation of extra-framework Al species [29, 69, 70]. The dealumination is prevented by the preparation of H-form zeolite from NH_4-form just before use without exposure to atmosphere [69, 71].

Partially ion-exchanged samples were prepared by varying the amount of NH_4NO_3, and termed HNaK-YNU-5.

Dealumination was performed according to the previous report [41]. The treatment conditions, and the obtained results are summarized in Table 1. Reflux of the calcined YNU-5 in 2.0 mol dm^{-1} nitric acid using a hot oil bath (403 K) was adopted to replace a part of framework Al with Si as already reported [41], and the resulting dealuminated YNU-5 with high stability is designated as “stable deAl-YNU-5”. The mild heating (353 K) of YNU-5 in an acid was reported to give an unstable sample due to dealumination and formation of defects; the thus obtained sample is denoted “unstable deAl-YNU-5”. Treatment with concentrated nitric acid gave the sample named “deeply-deAl-YNU-5” with very low aluminum content [Al] in mole per kilogram sample. The

chemical compositions including [Al] were analyzed by inductively coupled plasma atomic emission spectroscopy (ICP-AES) and presented in Table 1.

The YNU-5 samples prepared under the given conditions have been confirmed to have **YFI** framework, high crystallinity and high micropore volume [39-41]. For the sake of comparison, zeolites with **FAU**, **MFI**, ***BEA**, **MWW** and **MOR** frameworks (Table S1) were also employed.

Ammonia IRMS-TPD measurements were performed according to our previous paper [17, 23]. The IR spectra of YNU-5 type samples (Figure S3) and ammonia TPD profiles of Brønsted acid sites on various YNU-5 samples and other types of zeolites (Figure S4) are shown in the Supporting Information. For pyridine adsorption experiments followed by the ammonia adsorption, a self-supported disc was prepared and after activation, the pyridine was adsorbed at 343 K. Then, ammonia was introduced at 343 K, and the sample was heated from 343 to 823 K with recording IR. Independently, the IR spectrum of adsorbed pyridine was collected after pretreatment of the sample at 723 K, adsorption of pyridine at 423 K to quantify the Brønsted and Lewis acid sites based on the reported molar extinction coefficient [66]. Similar pretreatment prior to the adsorption of CD_3CN was used; the IR spectra were recorded and analyzed based on the reported molar extinction coefficient [67].

Quantum chemical calculations of ammonia desorption energy/enthalpy were carried out based on density functional theory (DFT) using a $Dmol^3$ software developed by BIOVIA in periodic boundary conditions using the (HCTH) 407 correlation-exchange functional [72], as detailed in Supporting Information. In our previous paper, agreement between the experimentally observed ΔH values and those calculated by principally same method have been reported [35]. The calculations were performed for the H-form zeolite model with a pair of H and Al atoms at all crystallographically non-equivalent positions in one unit cell of the **YFI** framework. The structure

optimization was carried out for the H-form and corresponding NH_4-form models. The molar standard energy/enthalpy of ammonia desorption was calculated from

$$\Delta U = U_{\text{H-Z}} + U_{\text{NH}_3\text{(g)}} - U_{\text{NH}_4\text{-Z}}$$

where ΔU showed the standard molar energy of ammonia desorption, U_x showed the total energy of species x, and -Z showed the zeolite anion, and

$$\Delta H = \Delta U + P\Delta V = \Delta U + RT \approx \Delta U + 5 \text{ kJ mol}^{-1}$$

where ΔH showed the standard molar enthalpy of ammonia desorption, P showed the pressure of standard conditions (10^5 Pa), ΔV showed the volume increase by the desorption of ammonia in standard conditions ($\approx RT$), R showed the gas constant, and T showed the average temperature of experiments (ammonia desorption); on approximation T = 600 K gives RT = 5 kJ mol^{-1}.

The energy calculations were also performed for models possessing one Al atom and one negative charge in one unit cell with all 9 crystallographically non-equivalent positions of Al without counter cation, as well as the energies of the **YFI** framework with one Si vacancy replaced by four OH groups forming silanol nest (Figure S2) were calculated according to Petkov et al [73]. The same approach has been used to calculate the energy gain for substitution of Si with Al (replacement of Si with Al) in the zeolite. We started with an all-silica model of **YFI** zeolite framework using a unit cell with the following dimensions a = 1.81807 nm, b = 3.18406 nm, c = 1.26407 nm, and symmetry corresponding to the space group *Cmmm*. The relative energy, ΔE, for the formation of silanol nest in each T-atom positions of the **YFI** framework is calculated at the reaction energy of the following formal reaction:

$$Zeo[(SiO_2)_n] + 4H_2O \rightarrow Zeo[(Si_{n-1}O_{2n}H_4)] + Si(OH)_4.$$

All reported energies are obtained for fully relaxed structures. A negative value of the substitution energies ΔE suggests that the formation of the silanol nest in the corresponding position or the replacement of Si with Al is preferable, while a positive value corresponds to unfavorable substitution. Those energy values give estimates of the relative preference for substitution in different crystallographic positions in the framework, as already reported for Ti-silicates [74] or Ge-silicates [73].

Results

Brønsted acid amount and strength

Figure 2 displays the Brønsted (filled symbols) and Lewis (open symbols) acid amounts estimated by ammonia IRMS-TPD (blue symbols), pyridine IR (green symbols) and CD_3CN IR (purple symbols). One can find that the three methods exhibited similar values throughout the cases where the three methods were applied to one sample. The Brønsted acid amount showed a linear relationship with [Al]−[Na]−[K], and the values were slightly lower than [Al]−[Na]−[K] over the HNaK-YNU-5 (partially ion-exchanged samples), H-YNU-5 (completely ion-exchanged sample) and dealuminated samples. This indicates that, principally, the isomorphous substitution of one tetravalent Si atom with a trivalent Al atom in the framework generated one Brønsted acid site, and that most of Al atoms were incorporated into the framework, as often found in zeolites with high crystallinity [17]. In contrast, none or only a few Lewis acid sites were observed, supporting that most Al atoms were in the framework position and acted as Brønsted acid sites.

The number of Brønsted acid sites on “unstable deAl-YNU-5” was lower than on the “stable deAl-YNU-5”, although Al content was similar to that in the “stable deAl-YNU-5”, indicating that the destruction of the framework was more significant in the “unstable deAl-YNU-5”, as already reported [41]. The deeply dealuminated sample (“deeply-deAl-YNU-5”) exhibits a few acid sites, due to the very low Al content.

The experimentally observed Brønsted acid strength distribution revealed by the ammonia desorption enthalpy (ΔH) is presented in Figure 3. Only on **MOR**, the acidic properties of Brønsted acidic OH groups in 8-ring and 12-ring are separately analyzed [23], because they have different wavenumbers in the IR spectrum [18-20, 75]. ΔH of 71% of Brønsted acid sites in H-YNU-5 was within 140 − 170 kJ mol^{-1} range. The Brønsted acid strength of the series of **YFI** samples with different aluminum content was as follows: the ΔH distribution of the H-YNU-5 and unstable deAl-YNU-5 showed weaker sites in the range 110 − 140 kJ mol^{-1}, while that of the stable deAl-YNU-5 was relatively sharp with 140 − 165 kJ mol^{-1} values.

Figure 3 shows ΔH distributions on zeolites with various framework topologies; the samples were chosen from a range of aluminum content 1 − 2 mol kg^{-1}. The ΔH on **FAU** was distributed in 100 − 150 kJ mol^{-1} with ca. 125 kJ mol^{-1} of the top of the distribution curve. The **MOR** (12-ring) showed slightly higher ΔH in a range of 100 − 150 kJ mol^{-1} with the top at ca. 140 kJ mol^{-1}. The ***BEA** also revealed ΔH in a range of 100 − 150 kJ mol^{-1} with the top at ca. 140 kJ mol^{-1}. Compared to these 12-ring zeolites (**FAU** and ***BEA**) or the Brønsted acid sites located in 12-rings (**MOR**), the 10-ring zeolites, i.e., **MFI** and **MWW**, revealed the higher regions of ΔH; the **MFI** showed mainly 130 − 150 kJ mol^{-1} of ΔH with ca. 140 kJ mol^{-1} of the top of distribution curve, whereas the **MWW** showed a broader distribution over 100 − 180 kJ mol^{-1} of ΔH with ca. 150 kJ mol^{-1} of the top. The ΔH of Brønsted acid sites in 8-ring of **MOR** was in 150 − 180 kJ mol^{-1} with the top at 170 kJ mol^{-1}, being highest among the examined zeolites. Compared with these

zeolites, the ΔH observed on **YFI**, 140 − 170 kJ mol^{-1} range as stated above, was obviously higher than **FAU** and ***BEA**, similar to **MWW** and located between **MFI** and **MOR** (8-ring). In other words, the order of the ΔH of Brønsted acid sites was **FAU** < **MOR** (12-ring) ≈ ***BEA** < **MFI** < **MWW** ≈ **YFI** < **MOR** (8-ring). It is noteworthy that the **YFI** (YNU-5 type zeolite) exhibited the highest ΔH among the 12-ring zeolites.

Accessibility of Brønsted acid sites

The H-YNU-5 showed a large absorption band ascribed to the stretching of Brønsted acidic OH groups at 3610 cm^{-1} [Figure 4 (A)]. A small absorption at 3745 cm^{-1} due to isolated SiOH groups was observed similarly to highly siliceous middle or large pore zeolites such as **MFI** [76] and ***BEA** [77, 78]. Here it is noteworthy that the OH stretching band was single. After elimination of the influences by the external surface, extra-framework species and defect, the **MFI** zeolite shows single acidic OH stretching band like the present **YFI** [79], while the **MOR** shows a band with a broad tail extended to the lower wavenumber region [20, 23]. Origin of the separation or broadening of the band on **MOR** has been analyzed to be the position of acidic OH group; the OH groups in 8- and 12-rings show the bands at ca. 3585 and 3615 cm^{-1}, respectively [20, 80]. The reason for the single band on **MFI** is believed to that most of acidic OH groups are in 10-ring. Based on these knowledges, it is considered that the acidic OH groups in YNU-5 behaves as if they are in the same size of micropore, although the **YFI** framework structure has 12-12-8-ring system and isolated 8-ring.

The Brønsted acidic OH groups were almost completely attenuated by the contact with pyridine vapor (B), clearly indicating that most of the Brønsted acid sites on the H-YNU-5 zeolite were accessible by pyridine. Simultaneously, pyridinium cations were detected through their characteristic band at 1540 cm^{-1} [Figure 5 (b)] [81], as already reported [39], evidencing the

neutralization of Brønsted acid sites by the base (pyridine). In addition, absorption bands were observed at 1445 and 1455 cm^{-1}, attributed to hydrogen-bonded and Lewis acid-coordinated pyridine, respectively. The latter was small, in agreement with a small amount of Lewis acid sites detected by the ammonia IRMS-TPD method.

Then, ammonia was introduced at 343 K. The adsorption temperature was chosen to be sufficiently low to allow all the Brønsted acid sites with ΔH > 100 kJ mol^{-1} holding ammonia. It was observed that the introduction of ammonia into the system did not largely change the spectrum in the OH stretching region (3500−3800 cm^{-1}) [Figure 4 (C)], indicating the absence of Brønsted acid sites which are accessible solely for ammonia but not for pyridine. The band due to pyridinium cation at 1540 cm^{-1} and other absorption bands due to adsorbed pyridine or pyridinium cation (1640, 1630, 1590 and 1480 cm^{-1}) were slightly weakened but not largely affected by the contact with ammonia. On the other side, the absorbance in 1400−1500 cm^{-1} region [Figure 5 (c0)], which was in agreement with the symmetric deformation of ammonium cation [52], was observed after the introduction of ammonia. It suggests that a part of pyridinium bonded to the Brønsted acid sites was replaced by ammonium cation; it just tells us the accessibility of these Brønsted acid sites by both pyridine and ammonia. The bands ascribed to the adsorbed pyridine (including pyridinium cation) and ammonium cation gradually decreased with the raise of the temperature [(c1)−(c5)].

The stable deAl-YNU-5 showed a band of Brønsted acidic OH groups at 3610 cm^{-1} overlapping a broad absorption due to SiOH (and possibly AlOH) with various environments around 3650−3745 cm^{-1} region [Figure 6 (A)]. Upon saturation with pyridine, the acidic OH band disappear [Figure 7 (b)], which is a consequence of the formation of pyridinium cation. This result again indicates that Brønsted acid sites are fully accessible. In addition, the contact with pyridine modified the shape of the free OH band peak around 3745 cm^{-1}, presumably due to the hydrogen-bonding between pyridine and OH [21]. The introduction of ammonia after these

procedures changed the shape of the broad OH band, but never changed the spectrum around 3600 cm^{-1} [Figure 6 (C)], indicating the lack of Brønsted acid sites accessible for ammonia but not for pyridine. After the adsorption of pyridine, the band of hydrogen-bonded pyridine (1445 cm^{-1}) was more intense on this sample [Figure 7 (c0)]. The heating even at 473 K removed most of the 1445 cm^{-1}-band [Figure 7 (c2)], supporting that the attribution of this band to the hydrogen-bonded species (weakly-held compared to the species with acid-base interaction).

The unstable deAl-YNU-5 showed only a weak intensity of the band ascribed to the stretching vibration of Brønsted acidic OH group, overlapping the large band due to SiOH (and possibly AlOH) with various environments [Figure 8 (A)]. The band ascribed to the hydrogen-bonded pyridine was larger than that on the stable deAl-YNU-5 [Figure 9 (b)]. The OH group concentration formed by the acid treatment for dealumination on the unstable deAl-YNU-5 was presumably higher than that on the stable deAl-YNU-5. The Brønsted acidic OH group was observed to lose intensity by the contact with pyridine, indicating that most of the Brønsted acid sites on this sample were also accessible by pyridine. The spectrum of Brønsted acidic OH was unchanged upon further contact with ammonia, showing the lack of Brønsted acid sites accessible only by ammonia but not by pyridine also on this sample.

Calculated ammonia desorption enthalpy

As shown in Table 2, most protons located at crystallographically non-equivalent positions in the **YFI** framework are estimated to possess 110 − 170 kJ mol^{-1} of ΔH. In Figure 10, the positions where protons show strong Brønsted acidity (ΔH > 140 kJ mol^{-1}) are displayed by red dots, and the blue dots show the positions where protons reveal weak Brønsted acidity (ΔH < 140 kJ mol^{-1}). Most of the red dots are located in the 8-rings, whereas most blue dots are in the 12-rings. On the other hand, Figure 11 indicates that ΔH of Brønsted acid sites in the isolated 8-ring,

connected 8-ring and 12-ring mainly distribute in 140 − 170, 130 − 140 and 110 − 130 kJ mol^{-1}, respectively. These tell us a tendency that the strong Brønsted acid sites are generated in small pores, in agreement with the observations in the previous section. In addition, it is estimated that the Brønsted acid sites with ΔH < 140 kJ mol^{-1} are located in the 12-12-8-ring system (12-ring and connected 8-ring), whereas the sites with ΔH > 140 kJ mol^{-1} are located in the isolated 8-ring.

The deprotonation energies [62, 63] of these sites are of interest, but we have not investigated. The calculation of deprotonation energy has still been influenced by charge localization, and accurate evaluation requires a broad range of trials [63]. This study adopted a method for calculation of ΔH which is similar to our previous study, and the agreement with the experimental observations has been confirmed [35]. We here discuss on only ΔH, and the deprotonation energy will be investigated in future.

Energies of dealumination

The dealumination of **YFI** framework with 120 T atoms in the unit cell, among which one site is occupied by the Al atom, is expected to proceed via the following chemical formulas:

$$Zeo[(SiO_2)_{119}(AlO_2)_1]^- + H^+ + 3H_2O \rightarrow Zeo[Si_{119}O_{240}H_4] + Al(OH)_3 \quad (1)$$

$$Zeo[(SiO_2)_{119}(AlO_2)_1]^- + H^+ + Si(OH)_4 \rightarrow Zeo[(SiO_2)_{120}] + Al(OH)_3 + H_2O \quad (2)$$

where Zeo[x] means the **YFI** framework with x representing the composition; $Zeo[(SiO_2)_{119}(AlO_2)_1]^-$ shows the framework with an Al atom and a negative charge in one unit cell; $Zeo[Si_{119}O_{240}H_4]$ shows the framework with a vacancy shown by Figure S2 in one unit cell; $Zeo[(SiO_2)_{120}]$ shows the completely siliceous framework. The dealumination may terminate to

form the vacancy by the reaction (1), while, in some different set of conditions, healing the vacancy with migration of Si species may occur to complete the total reaction formula (2).

Table 2 shows the relative energy of $Zeo[(SiO_2)_{119}(AlO_2)_1]^-$, which corresponds to the energy for the inverse of the reaction (2). Low values (0−7 kJ mol^{-1}) at T1, T2, T4, T5 and T6 suggest difficulty of the dealumination with migration of Si species at these positions. In addition, the calculated energies for the Si vacancy formation [energies of the reaction (1)] are also listed in Table 2. It ranges from −67 to +8 kJ mol^{-1}. The high values at T4 and T5 sites (−2 kJ mol^{-1} and 8 kJ mol^{-1}, respectively) suggest that the dealumination resulting in the formation of silanol nests at these positions is not preferred. The energy at T1 (−18 kJ mol^{-1}) was also higher than other sites. The large negative values imply that the removal of Al is a spontaneous process at the sites other than T1, T4 and T5. From these calculations, we estimate that the dealumination is relatively difficult at T1, T4 and T5 positions in the **YFI** framework. The T1 and T4 are the positions inside the isolated 8-ring with no oxygen atoms sharing with 12-12-8-ring system.

Discussion

Presence of Brønsted acid sites with high ammonia desorption enthalpy accessible from 12-12-8-ring system

The 10-ring in **MFI** allows diffusion of benzene derivatives and small alkanes, but the adsorption/diffusion of polycyclic aromatics like naphthalene and bulky branched alkanes is difficult. **MWW** framework has large cavities, but they are isolated and connected by 10-ring windows, which allows the diffusion of only molecules smaller than 10-ring. **FAU**, **MOR**, ***BEA** and **YFI** have 12-ring systems which enable large molecules such as branched alkanes and polycyclic aromatics to diffuse inside. As one of the parameters showing the strength of acid-base

interaction due to the Brønsted acid site on solids, ΔH (ammonia desorption enthalpy) of these framework structures were found in the order of **FAU** < **MOR** (12-ring) ≈ ***BEA** < **MFI** < **MWW** ≈ **YFI** < **MOR** (8-ring) (Figure 3). The Brønsted acid sites in 12- and 8-rings of **MOR** are identified by their IR wavenumber [20], as the strong acid sites are located only in the 8-ring [23], in agreement with previous studies [20, 22]. On the other hand, most of the Brønsted acid sites in **YFI** type zeolite were observed to be accessible by pyridine. This was observed on all of the H-YNU-5 and dealuminated samples (Figures 4−9). The molecular size of pyridine (0.57 nm) [82] is obviously larger than the 8-ring of **YFI** (0.36 nm) [7], and therefore, pyridine is presumed to access the Brønsted acid sites from the 12-12-8-ring system side. These observations indicate that the Brønsted acid sites with high ammonia desorption enthalpy in YNU-5 zeolite are accessible from the large micropore (12-12-8-ring system). More precisely, the Brønsted acid sites in YNU-5 zeolite located in 12-12-8-ring system and isolated 8-ring both react with pyridine. As stated above, the ammonia desorption enthalpy of YNU-5 type zeolite was higher than those in 12-rings of **FAU**, **MOR** and ***BEA**, and higher or comparable to those on the 10-ring zeolites, i.e., **MFI** and **MWW**. From a view of ammonia desorption enthalpy, Brønsted acid sites on **YFI** showed the highest value among those accessible from 12-ring to the best of our knowledge.

Because the number of Brønsted acid sites in the series of **YFI** discussed here were approximately equal to the number of ion exchange sites based on chemical composition [Al]−[Na]−[K] (Figure 2), the above nature of Brønsted acid sites is believed be due to the intrinsic property of **YFI** framework but not by exceptional phenomena due to impurity, extra-framework metal species nor defects.

Positions of Brønsted acid sites

Nakazawa et al. reported that at counter cations (mainly K^+), at least a part of them, are located in the isolated 8-ring of as-synthesized YNU-5 zeolite [39]. Consequently, after the conversion of zeolite in H-form, at least a part of generated protons is located in the isolated 8-ring. The latter suggestion is in line with the quantum chemical calculations showing that the Brønsted acid sites with ΔH > 140 kJ mol^{-1} are located in the 8-rings (Figure 11). In conclusion, it is reasonable to say that most of the Brønsted acid sites with high ammonia desorption enthalpy were located in the 8-rings before contact with pyridine.

It is known that the protons hop on the four oxygen atoms bonded to Al (ion exchange site) [83-86] with the activation energy <40 kJ mol^{-1} [87], sufficiently low for the free movement at 343 K where the adsorption of pyridine was performed in the present study. It is probable that a part of the Brønsted acidic protons were originally located in the 8-ring and moved to react with pyridine through the monoatomic thickness silicate wall between the isolated 8-ring and 2-dimensional 12-ring system.

It is known that the OH groups in 8- and 12-rings of **MOR** show the bands at ca. 3585 and 3615 cm^{-1}, respectively, and the former is not accessible by pyridine [20, 80]. In contrast, a single band was observed due to the stretching vibration of acidic OH groups on YNU-5, although the acidic OH groups of **YFI** should be also distributed in 8- and 12-rings. The hopping of protons should delocalize their positions to show a single vibration band in the IR spectrum, and therefore the above explanation that the proton hopping contributed to the accessibility of bulky molecule is supported.

Dealumination behavior

The experimental results pointed out that ΔH of the Brønsted acid sites on the **YFI** type zeolites were distributed in 110 − 170 kJ mol^{-1} range (Figure 3). The quantum calculations estimate the total distribution of ΔH is in a range of 110 − 170 kJ mol^{-1} (Table 2). Thus, the experiments agreed with the calculations form a view of ΔH.

The quantum calculations furthermore derive the ΔH distributions in the isolated 8-ring, connected 8-ring and 12-ring mainly distribute in 140 − 170, 130 − 140 and 110 − 130 kJ mol^{-1}, respectively (Figure 11). In other words, the Brønsted acid sites in the 12-12-8-ring system (12-ring and connected 8-ring) should possess ΔH < 140 kJ mol^{-1}, whereas the sites in the isolated 8-ring should show ΔH > 140 kJ mol^{-1}. The experiments indicated that the H-YNU-5 zeolite showed the ΔH distribution over 110 − 170 kJ mol^{-1}, while the stable deAl-YNU-5 had only the Brønsted acid sites with ΔH > 140 kJ mol^{-1} (Figure 3). In detail, because the Brønsted acid sites was largely decreased over a wide range of ΔH by the dealumination from the H-YNU-5 into stable deAl-YNU-5, it is considered that the dealumination proceeded in both 12-12-8-ring system and isolated 8-ring. However, the resultant stable deAl-YNU-5 showed negligible amount of the Brønsted acid sites with ΔH < 140 kJ mol^{-1}, indicating that the remaining Brønsted acid sites were mainly located in the isolated 8-ring. This suggests that the dealumination preferentially occurred in the 12-12-8-ring system. The quantum calculations show the difficulty of dealumination at T1, T4 and T5 positions in the **YFI** framework. The T1 and T4 are the positions inside the isolated 8-ring with no oxygen atoms sharing with 12-12-8-ring system, and therefore, this supports that the Brønsted acid sites in the isolated 8-ring survived the dealumination, and the thermodynamic stability was the reason for preferential dealumination.

Removal of Al from both 12-12-8-ring system and isolated 8-ring on the initial stage of dealumination can explain the previously observed behaviors of degradation and selectivity in dimethyl ether-to-olefin reaction on the dealuminated **YFI** zeolite [39, 41, 42]. The high catalytic

activity for the reaction of YNU-5 zeolite with high [Al] (corresponding to the H-YNU-5 in the present study) quickly dropped by heavy coke formed at mainly opened spaces such as external surface and 12-ring. This type of degradation of catalyst was prevented by dealumination resulting in a moderate Si/Al ratio to reduce the active site concentration [39], in agreement with removal of Al from both 12-12-8-ring system and isolated 8-ring observed from the present H-YNU-5 into stable deAl-YNU-5. A different type of relatively slow catalyst deactivation was observed, probably due to coke formation even in small spaces plugging the isolated ring. The slow deactivation was observed up to very high Si/Al ratio 160 [39]. This agrees with the present finding that the remaining Al was mainly in the isolated 8-ring on the stable deAl-YNU-5 sample with Si/Al > ca. 50. A stable activity was found at Si/Al = ca. 60 after the slow deactivation was saturated (probably due to the complete blocking of the isolated 8-ring) [39]. The stable activity is believed to be due to the reaction in the 12-12-8-ring system, because the product distribution was similar to that on ***BEA** zeolite (beta) with 12-12-12-ring system but far from **CHA** (SSZ-13) with the 8-8-8-ring [42]. It is speculated that the hydrocarbons accessed from the 12-12-8-ring system to the Brønsted acid sites remaining in the isolated 8-ring; this agrees with the presently observed accessibility of a bulky molecule to the Brønsted acid sites which were estimated to be in the isolated 8-ring.

On the other hand, the unstable deAl-YNU-5 zeolite showed a wide ΔH distribution over 110−170 kJ mol^{-1}, while the stable deAl-YNU-5 with similar Si/Al ratio showed ΔH > 140 kJ mol^{-1} and hence the position of Brønsted acid sites was the isolated 8-ring as above according to the thermodynamic stability. It is speculated that kinetics or mass transfer influenced on the extent of reaction at the lower temperature (353 K) adopted for dealumination of the unstable sample, whereas the equilibrium was achieved to reach the structure controlled by the thermodynamic stability at the higher temperature (reflux conditions in 403 K oil bath) for the stable sample. For example, difficulty of the dealumination inside the particle (crystallite or secondary particle) of

zeolite is speculated to result in the high extent of dealumination only in the external surface region at the lower temperature.

Conclusion

The acidic property of YNU-5 zeolite with a unique 12−12−8-ring system was studied. A combination of IR analysis using multiple probe molecules, ammonia IRMS-TPD techniques and molecular modeling was employed to evaluate the acid site strength, distribution, and accessibility. No or negligible amount of Lewis acid sites was detected. The agreement was observed between the numbers of Brønsted acid sites and Al atoms, and therefore the following results are believed to show the nature of bridging Si(OH)Al group in the **YFI** framework.

The IR band due to the stretching vibration of Brønsted acidic OH groups was almost completely diminished by the contact with pyridine vapor to form pyridinium cations. Further introduction of ammonia did not largely change the spectrum of OH stretching region, indicating that most of the Brønsted acid sites are accessible by pyridine. The ammonia desorption enthalpy was observed to distribute over a range of 100−170 kJ mol^{-1}. Previous studies indicated the presence of counter cations in the isolated 8-ring of alkaline form of YNU-5 zeolite, and the DFT calculations show that the Brønsted acidic protons with ammonia desorption enthalpy > 140 kJ mol^{-1} are mainly located in the isolated 8-ring. Pyridine molecule, which is larger than the 8-ring, is therefore speculated to access to the Brønsted acid sites in the isolated 8-ring from the 12-12-8-ring system side, probably through the hopping of proton beyond the thin silicate wall separating the 12-12-8-ring system and isolated 8-ring.

The ammonia desorption enthalpy, which can be an index of acid strength or reactivity of the acid site with a basic reactant, was in the following order: **FAU** < **MOR** (12-ring) ≈ ***BEA** <

MFI < **MWW** ≈ **YFI** < **MOR** (8-ring); in the case of **MOR**, the Brønsted acid sites in 12- and 8-rings were individually analyzed because they showed different wavenumbers in the IR spectrum. Thus, marked ammonia desorption enthalpy on the **YFI** zeolite compared to the other 12-ring zeolites was observed.

The dealumination at a high temperature under the reflux conditions with nitric acid, which leads the stabilization through migration of Si to the silanol nest, resulted in the preferential removal of Brønsted acid sites from the 12-12-8-ring system. This explains well the previously reported catalytic properties of YNU-5 zeolite for dimethyl ether-to-olefin reaction.

Appendix

Supplementary data to this article can be found online. It includes further details concerning the experimental procedures for zeolite synthesis, several characterizations, such as ammonia IRMS-TPD as well as FT-IR using probe molecules, quantum chemical calculations. List of reference samples, partial drawings of the **YFI** framework showing T sites, schematic illustration of silanol nest in the zeolite framework, IR spectra of adsorbed ammonia, ammonia TPD profiles of Brønsted acid sites, IR spectra of adsorbed pyridine, and IR spectra of adsorbed CD_3CN are also shown.

Author Information

Corresponding Author

*E-mail: katada@tottori-u.ac.jp (N. K.), kubota-yoshihiro-sr@ynu.ac.jp (Y. K.)

Funding

A part of this study was supported by CREST (Grant Number JPMJCR17P1) and EIG CONCERT-Japan program (Grant Number JPMJSC18C4), the Japan Science and Technology Agency (JST), and KAKENHI (Grant Number 16H04568 and 21H01717), the Japan Society for the Promotion of Science (JSPS), Japan. A part of the results was obtained in the framework of JPNP20012 project, subsidized by the New Energy and Industrial Technology Development Organization (NEDO). PStP and KS are supported by Bulgarian Science Fund (Grant Number KP-06-DO02/2).

References

[1] D.W. Breck, Zeolite Molecular Sieves: Structure, Chemistry, and Use, Wiley1974.

[2] A. Palcic, V. Valtchev, Analysis and control of acid sites in zeolites, Appl. Catal. A: Gen., 606 (2020) 117795, https://doi.org/10.1016/j.apcata.2020.117795.

[3] D. Kerstens, B. Smeyers, J. Van Waeyenberg, Q. Zhang, J.H. Yu, B.F. Sels, State of the Art and Perspectives of Hierarchical Zeolites: Practical Overview of Synthesis Methods and Use in Catalysis, Adv. Mater., 32 (2020) 2004690, https://doi.org/10.1002/adma.202004690.

[4] J.Y. Li, A. Corma, J.H. Yu, Synthesis of new zeolite structures, Chem. Soc. Rev., 44 (2015) 7112-7127, https://doi.org/10.1039/c5cs00023h.

[5] A. Deneyer, Q.L. Ke, J. Devos, M. Dusselier, Zeolite Synthesis under Nonconventional Conditions: Reagents, Reactors, and Modi Operandi, Chem. Mater., 32 (2020) 4884-4919, https://doi.org/10.1021/acs.chemmater.9b04741.

[6] M. Hartmann, M. Thommes, W. Schwieger, Hierarchically-Ordered Zeolites: A Critical Assessment, Adv. Mater. Interfaces, 8 (2021) 2001841, https://doi.org/10.1002/admi.202001841.

[7] C. Baerlocher, L.B. McCusker, Database of Zeolite Structures, Database of Zeolite Structures.

[8] A. Corma, Inorganic Solid Acids and Their Use in Acid-Catalyzed Hydrocarbon Reactions, Chem. Rev., 95 (1995) 559-614, https://doi.org/10.1021/cr00035a006.

[9] M. Shamzhy, M. Opanasenko, P. Concepcion, A. Martinez, New trends in tailoring active sites in zeolite-based catalysts, Chem. Soc. Rev., 48 (2019) 1095-1149, https://doi.org/10.1039/c8cs00887f.

[10] A.K. Mostafazadeh, O. Solomatnikova, P. Drogui, R.D. Tyagi, A review of recent research and developments in fast pyrolysis and bio-oil upgrading, Biomass Convers. Bior., 8 (2018) 739-773, https://doi.org/10.1007/s13399-018-0320-z.

[11] X.W. Chi, M.L. Li, J.C. Di, P. Bai, L.N. Song, X.X. Wang, F. Li, S. Liang, J.J. Xu, J.H. Yu, A highly stable and flexible zeolite electrolyte solid-state Li-air battery, Nature, 592 (2021) 551-570, https://doi.org/10.1038/s41586-021-03410-9July2020.

[12] A. Arora, M.M.F. Hasan, Flexible oxygen concentrators for medical applications, Sci. Rep., 11 (2021) 14317, https://doi.org/10.1038/s41598-021-93796-3.

[13] L. Bacakova, M. Vandrovcova, I. Kopova, I. Jirka, Applications of zeolites in biotechnology and medicine - a review, Biomater. Sci., 6 (2018) 974-989, https://doi.org/10.1039/c8bm00028j.

[14] S. Kotrel, M.P. Rosynek, J.H. Lunsford, Intrinsic catalytic cracking activity of hexane over H-ZSM-5, H-beta and H-Y zeolites, J. Phys. Chem. B, 103 (1999) 818-824, https://doi.org/10.1021/jp982538l.

[15] N. Katada, H. Igi, J.H. Kim, M. Niwa, Determination of the acidic properties of zeolite by theoretical analysis of temperature-programmed desorption of ammonia based on adsorption equilibrium, J. Phys. Chem. B, 101 (1997) 5969-5977, https://doi.org/10.1021/jp9639152.

[16] N. Katada, K. Suzuki, T. Noda, W. Miyatani, F. Taniguchi, M. Niwa, Correlation of the cracking activity with solid acidity and adsorption property on zeolites, Appl. Catal. A: Gen., 373 (2010) 208-213, https://doi.org/10.1016/j.apcata.2009.11.022.

[17] N. Katada, Analysis and interpretation of acidic nature of aluminosilicates, Mol. Catal., 458 (2018) 116-126, https://doi.org/10.1016/j.mcat.2017.12.024.

[18] P.A. Jacobs, W.J. Mortier, An Attempt to Rationalize Stretching Frequencies of Lattice Hydroxyl-Groups in Hydrogen-Zeolites, Zeolites, 2 (1982) 226-230, https://doi.org/10.1016/S0144-2449(82)80056-0.

[19] M. Maache, A. Janin, J.C. Lavalley, E. Benazzi, Ft Infrared Study of Bronsted Acidity of H-Mordenites - Heterogeneity and Effect of Dealumination, Zeolites, 15 (1995) 507-516, https://doi.org/10.1016/0144-2449(95)00019-3.

[20] A. Alberti, Location of Bronsted sites in mordenite, Zeolites, 19 (1997) 411-415, https://doi.org/10.1016/S0144-2449(97)00114-0.

[21] J. Datka, B. Gil, A. Kubacka, Heterogeneity of OH groups in H-mordenites: Effect of dehydroxylation, Zeolites, 17 (1996) 428-433, https://doi.org/10.1016/S0144-2449(96)00009-7.

[22] V.L. Zholobenko, M.A. Makarova, J. Dwyer, Inhomogeneity of Bronsted Acid Sites in H-Mordenite, J. Phys. Chem., 97 (1993) 5962-5964, https://doi.org/10.1021/j100124a030.

[23] M. Niwa, K. Suzuki, N. Katada, T. Kanougi, T. Atoguchi, Ammonia IRMS-TPD study on the distribution of acid sites in mordenite, J. Phys. Chem. B, 109 (2005) 18749-18757, https://doi.org/10.1021/jp051304g.

[24] K. Suzuki, N. Katada, M. Niwa, Detection and quantitative measurements of four kinds of OH in HY zeolite, J. Phys. Chem. C, 111 (2007) 894-900, https://doi.org/10.1021/jp065054v.

[25] C.T. Kresge, M.E. Leonowicz, W.J. Roth, J.C. Vartuli, J.S. Beck, Ordered Mesoporous Molecular-Sieves Synthesized by a Liquid-Crystal Template Mechanism, Nature, 359 (1992) 710-712, https://doi.org/10.1038/359710a0.

[26] S. Inagaki, Y. Fukushima, K. Kuroda, Synthesis of Highly Ordered Mesoporous Materials from a Layered Polysilicate, J. Chem. Soc. Chem. Comm., (1993) 680-682, https://doi.org/10.1039/c39930000680.

[27] A. Corma, Q.B. Kan, M.T. Navarro, J. PerezPariente, F. Rey, Synthesis of MCM-41 with different pore diameters without addition of auxiliary organics, Chem. Mater., 9 (1997) 2123-2126, https://doi.org/10.1021/cm970203v.

[28] S. Perez-Beltran, P.B. Balbuena, G.E. Ramirez-Caballero, Surface Structure and Acidity Properties of Mesoporous Silica SBA-15 Modified with Aluminum and Titanium: First-Principles Calculations, J. Phys. Chem. C, 120 (2016) 18105-18114, https://doi.org/10.1021/acs.jpcc.6b05630.

[29] N. Katada, Y. Kageyama, M. Niwa, Acidic property of Y- and mordenite-type zeolites with high aluminum concentration under dry conditions, J. Phys. Chem. B, 104 (2000) 7561-7564, https://doi.org/10.1021/jp000906r.

[30] P.A. Jacobs, W.J. Mortier, J.B. Uytterhoeven, Properties of Zeolites in Relation to Their Electronegativity - Acidity, Carboniogenic Activity and Strength of Interaction in Transition-Metal Complexes, J. Inorg. Nucl. Chem., 40 (1978) 1919-1923, https://doi.org/10.1016/0022-1902(78)80256-5.

[31] F. Lonyi, J.H. Lunsford, The Development of Strong Acidity in Hexafluorosilicate-Modified Y-Type Zeolites, J. Catal., 136 (1992) 566-577, https://doi.org/10.1016/0021-9517(92)90086-W.

[32] A. Corma, A. Martinez, C. Martinez, The role of extraframework aluminum species in USY catalysts during isobutane/2-butene alkylation, Appl. Catal. A: Gen., 134 (1996) 169-182, https://doi.org/10.1016/0926-860x(95)00228-6.

[33] K. Suzuki, T. Noda, G. Sastre, N. Katada, M. Niwa, Periodic Density Functional Calculation on the Bronsted Acidity of Modified Y-Type Zeolite, J. Phys. Chem. C, 113 (2009) 5672-5680, https://doi.org/10.1021/jp8104562.

[34] I.N. Senchenya, V.B. Kazansky, S. Beran, Quantum Chemical Study of the Effect of the Structural Characteristics of Zeolites on the Properties of Their Bridging Oh Groups .2., J. Phys. Chem., 90 (1986) 4857-4859, https://doi.org/10.1021/j100411a028.

[35] N. Katada, K. Suzuki, T. Noda, G. Sastre, M. Niwa, Correlation between Bronsted Acid Strength and Local Structure in Zeolites, J. Phys. Chem. C, 113 (2009) 19208-19217, https://doi.org/10.1021/jp903788n.

[36] N. Katada, K. Suzuki, T. Noda, M.B. Park, H.K. Min, S.B. Hong, M. Niwa, Ammonia IRMS-TPD Characterization of Bronsted Acid Sites in Medium-pore Zeolites with Different Framework Topologies, Top. Catal., 53 (2010) 664-671, https://doi.org/10.1007/s11244-010-9503-y.

[37] N. Katada, K. Nouno, J.K. Lee, J. Shin, S.B. Hong, M. Niwa, Acidic Properties of Cage-Based, Small-Pore Zeolites with Different Framework Topologies and Their Silicoaluminophosphate Analogues, J. Phys. Chem. C, 115 (2011) 22505-22513, https://doi.org/10.1021/jp207894n.

[38] T. Matsuoka, L. Baumes, N. Katada, A. Chatterjee, G. Sastre, Selecting strong Bronsted acid zeolites through screening from a database of hypothetical frameworks, Phys. Chem. Chem. Phys., 19 (2017) 14702-14707, https://doi.org/10.1039/c7cp01778b.

[39] N. Nakazawa, T. Ikeda, N. Hiyoshi, Y. Yoshida, Q. Han, S. Inagaki, Y. Kubota, A Microporous Aluminosilicate with 12-, 12-, and 8-Ring Pores and Isolated 8-Ring Channels, J. Am. Chem. Soc., 139 (2017) 7989-7997, https://doi.org/10.1021/jacs.7b03308.

[40] T. Ikeda, Y. Yoshida, N. Nakazawa, S. Inagaki, Y. Kubota, Solid-state NMR and powder X-ray diffraction studies on ammonium ion-exchanged and dealuminated zeolite YNU-5, Micropor. Mesopor. Mater., 302 (2020) https://doi.org/10.1016/j.micromeso.2020.110197.

[41] N. Nakazawa, Y. Yoshida, S. Inagaki, Y. Kubota, Synthesis of novel aluminosilicate YNU-5 and enhancement of the framework thermal stability by post-synthesis treatment, Micropor. Mesopor. Mater., 280 (2019) 66-74, https://doi.org/10.1016/j.micromeso.2019.01.004.

[42] Q. Liu, Y. Yoshida, N. Nakazawa, S. Inagaki, Y. Kubota, The Synthesis of YNU-5 Zeolite and Its Application to the Catalysis in the Dimethyl Ether-to-Olefin Reaction, Materials, 13 (2020) 2030, https://doi.org/10.3390/ma13092030.

[43] Q. Liu, R. Sugimoto, S. Inagaki, Y. Kubota, Introduction of Hierarchical Structure into YNU-5 Zeolite and Its Enhanced Catalytic Performance for Hexane Cracking, Chem. Lett., 50 (2021) 1725-1728, https://doi.org/10.1246/cl.210368.

[44] R.J. Cvetanović, Y. Amenomiya, Application of a Temperature-Programmed Desorption Technique to Catalyst Studies, Adv. Catal., 17 (1967) 103-149, https://doi.org/10.1016/s0360-0564(08)60686-0.

[45] M. Niwa, M. Iwamoto, K.I. Segawa, Temperature-Programmed Desorption of Ammonia on Zeolites - Influence of the Experimental Conditions on the Acidity Measurement, Bull. Chem. Soc. Jpn., 59 (1986) 3735-3739, https://doi.org/10.1246/bcsj.59.3735.

[46] R.J. Gorte, What do we know about the acidity of solid acids ?, Catal. Lett., 62 (1999) 1-13, https://doi.org/10.1023/a:1019010013989.

[47] W.L. Earl, P.O. Fritz, A.A.V. Gibson, J.H. Lunsford, A Solid-state NMR-study of Acid Sites in Zeolite-Y Using Ammonia and Trimethylamine as Probe Molecules, J. Phys. Chem., 91 (1987) 2091-2095, https://doi.org/10.1021/j100292a022.

[48] A. Zecchina, L. Marchese, S. Bordiga, C. Paze, E. Gianotti, Vibrational spectroscopy of NH4+ ions in zeolitic materials: An IR study, J. Phys. Chem. B, 101 (1997) 10128-10135, https://doi.org/10.1021/jp9717554.

[49] H. Igi, N. Katada, M. Niwa, Principle for Generation of Acidity in Y Zeolite Found by Ammonia Temperature-Programmed Desorption: Stoichiometric Generation of Acid Sites with a Constant Strength by Isolated Framework Al Atoms, Proceedings of the 12th International Zeolite Conference, (1999) 2643-2650.

[50] J. Valyon, G. Onyestyak, L.V.C. Rees, Study of the dynamics of NH_3 adsorption in ZSM-5 zeolites and the acidity of the sorption sites using the frequency-response technique, J. Phys. Chem. B, 102 (1998) 8994-9001, https://doi.org/10.1021/jp981872e.

[51] J. Valyon, G. Onyestyak, L.V.C. Rees, A frequency-response study of the diffusion and sorption dynamics of ammonia in zeolites, Langmuir, 16 (2000) 1331-1336, https://doi.org/10.1021/la990867e.

[52] S. Suganuma, Y. Murakami, J. Ohyama, T. Torikai, K. Okumura, N. Katada, Assignments of Bending Vibrations of Ammonia Adsorbed on Surfaces of Metal Oxides, Catal. Lett., 145 (2015) 1904-1912, https://doi.org/10.1007/s10562-015-1592-6.

[53] A.K. Ghosh, G. Curthoys, Characterization of Zeolite Acidity - an Infrared Study Using Ammonia, Methylamine and Normal-Butylamine, J. Chem. Soc. Faraday Trans. 1, 80 (1984) 99-109, https://doi.org/10.1039/f19848000099.

[54] M. Niwa, N. Katada, M. Sawa, Y. Murakami, Temperature-Programmed Desorption of Ammonia with Readsorption Based on the Derived Theoretical Equation, J. Phys. Chem., 99 (1995) 8812-8816, https://doi.org/10.1021/j100021a056.

[55] N. Naito, N. Katada, M. Niwa, Tungsten oxide monolayer loaded on zirconia: Determination of acidity generated on the monolayer, J. Phys. Chem. B, 103 (1999) 7206-7213, https://doi.org/10.1021/jp9906381.

[56] N. Katada, J. Endo, K. Notsu, N. Yasunobu, N. Naito, M. Niwa, Superacidity and catalytic activity of sulfated zirconia, J. Phys. Chem. B, 104 (2000) 10321-10328, https://doi.org/10.1021/jp002212o.

[57] M. Sawa, M. Niwa, Y. Murakami, Derivation of New Theoretical Equation for Temperature-programmed Desorption of Ammonia with Freely Occuring Readsorption, Zeolites, 10 (1990) 307-309, https://doi.org/10.1016/0144-2449(94)90147-3.

[58] M. Sawa, M. Niwa, Y. Murakami, One-point Method for Determining Acid Strength of Zeolite by Temperature-programmed Desorption of Ammonia, Zeolites, 11 (1991) 93-94, https://doi.org/10.1016/0144-2449(91)80400-t.

[59] N. Katada, T. Tsubaki, M. Niwa, Measurements of number and strength distribution of Bronsted and Lewis acid sites on sulfated zirconia by ammonia IRMS-TPD method, Appl. Catal. A: Gen., 340 (2008) 76-86, https://doi.org/10.1016/j.apcata.2008.01.033.

[60] L.P. Hammett, A.J. Deyrup, A Series of Simple Basic Indicators. I. The Acidity Functions of Mixtures of Sulfuric and Perchloric Acids with Watre1, J. Am. Chem. Soc., 54 (1932) 2721-2739, https://doi.org/10.1021/ja01346a015.

[61] M. Niwa, N. Katada, New Method for the Temperature-Programmed Desorption (TPD) of Ammonia Experiment for Characterization of Zeolite Acidity: A Review, Chem. Rec., 13 (2013) 432-455, https://doi.org/10.1002/tcr.201300009.

[62] M. Brandle, J. Sauer, Acidity differences between inorganic solids induced by their framework structure. A combined quantum mechanics molecular mechanics ab initio study on zeolites, J. Am. Chem. Soc., 120 (1998) 1556-1570, https://doi.org/10.1021/ja9729037.

[63] A.J. Jones, E. Iglesia, The Strength of Brønsted Acid Sites in Microporous Aluminosilicates, ACS Catal., 5 (2015) 5741-5755, https://doi.org/10.1021/acscatal.5b01133.

[64] K. Nakamura, R. Mizuta, S. Suganuma, E. Tsuji, N. Katada, Compensation between activation entropy and enthalpy in reactions of aromatic hydrocarbons catalyzed by solid acids, Catal. Commun., 102 (2017) 103-107, https://doi.org/10.1016/j.catcom.2017.08.033.

[65] N. Katada, S. Sota, N. Morishita, K. Okumura, M. Niwa, Relationship between activation energy and pre-exponential factor normalized by the number of Bronsted acid sites in cracking of short chain alkanes on zeolites, Catal. Sci. Technol., 5 (2015) 1864-1869, https://doi.org/10.1039/c4cy01483a.

[66] C.A. Emeis, Determination of Integrated Molar Extinction Coefficients for Infrared-Absorption Bands of Pyridine Adsorbed on Solid Acid Catalysts, J. Catal., 141 (1993) 347-354, https://doi.org/10.1006/jcat.1993.1145.

[67] B. Wichterlova, Z. Tvaruzkova, Z. Sobalik, P. Sarv, Determination and properties of acid sites in H-ferrierite - A comparison of ferrierite and MFI structures, Micropor. Mesopor. Mater., 24 (1998) 223-233, https://doi.org/Doi 10.1016/S1387-1811(98)00167-X.

[68] D. Barthomeuf, Topology and Maximum Content of Isolated Species (Al, Ga, Fe, B, Si, ...) in a Zeolitic Framework - An Approach to Acid Catalysis, J. Phys. Chem., 97 (1993) 10092-10096, https://doi.org/10.1021/j100141a032.

[69] N. Katada, T. Kanai, M. Niwa, Dealumination of proton form mordenite with high aluminum content in atmosphere, Micropor. Mesopor. Mater., 75 (2004) 61-67, https://doi.org/10.1016/j.micromeso.2004.07.001.

[70] N. Katada, T. Takeguchi, T. Suzuki, T. Fukushima, K. Inagaki, S. Tokunaga, H. Shimada, K. Sato, Y. Oumi, T. Sano, K. Segawa, K. Nakai, H. Shoji, P. Wu, T. Tatsumi, T. Komatsu, T. Masuda, K. Domen, E. Yoda, J.N. Kondo, T. Okuhara, Y. Kageyama, M. Niwa, M. Ogura, M. Matsukata, E. Kikuchi, N. Okazaki, M. Takahashi, A. Tada, S. Tawada, Y. Kubota, Y. Sugi, Y. Higashio, M. Kamada, Y. Kioka, K. Yamamoto, T. Shouji, Y. Arima, Y. Okamoto, H. Matsumoto,

Standardization of catalyst preparation using reference catalyst: ion exchange of mordenite type zeolite - 1. Remarkable dealumination accompanying ion exchange, Appl. Catal. A: Gen., 283 (2005) 63-74, https://doi.org/10.1016/j.apcata.2004.12.036.

[71] N. Katada, T. Takeguchi, T. Suzuki, T. Fukushima, K. Inagaki, S. Tokunaga, H. Shimada, K. Sato, Y. Oumi, T. Sano, K. Segawa, K. Nakai, H. Shoji, P. Wu, T. Tatsumi, T. Komatsu, T. Masuda, K. Domen, E. Yoda, J.N. Kondo, T. Okuhara, T. Kanai, M. Niwa, M. Ogura, M. Matsukata, E. Kikuchi, N. Okazaki, M. Takahashi, A. Tada, S. Tawada, Y. Kubota, Y. Sugi, Y. Higashio, M. Kamada, Y. Kioka, K. Yamamoto, T. Shouji, S. Satokawa, Y. Arima, Y. Okamoto, H. Matsumoto, Standardization of catalyst preparation using reference catalyst: ion exchange of mordenite type zeolite - 2. Origin of dealumination and recommended standard conditions, Appl. Catal. A: Gen., 283 (2005) 75-84, https://doi.org/10.1016/j.apcata.2005.01.026.

[72] A.D. Boese, N.C. Handy, A new parametrization of exchange-correlation generalized gradient approximation functionals, J Chem Phys, 114 (2001) 5497-5503, https://doi.org/10.1063/1.1347371.

[73] P.S. Petkov, H.A. Aleksandrov, V. Valtchev, G.N. Vayssilov, Framework Stability of Heteroatom-Substituted Forms of Extra-Large-Pore Ge-Silicate Molecular Sieves: The Case of ITQ-44, Chem. Mater., 24 (2012) 2509-2518, https://doi.org/10.1021/cm300861e.

[74] R.C. Deka, V.A. Nasluzov, E.A.I. Shor, A.M. Shor, G.N. Vayssilov, N. Rosch, Comparison of all sites for Ti substitution in zeolite TS-1 by an accurate embedded-cluster method, J. Phys. Chem. B, 109 (2005) 24304-24310, https://doi.org/10.1021/jp050056l.

[75] S.B. Sharma, B.L. Meyers, D.T. Chen, J. Miller, J.A. Dumesic, Characterization of Catalyst Acidity by Microcalorimetry and Temperature-Programmed Desorption, Appl. Catal. A: Gen., 102 (1993) 253-265, https://doi.org/10.1016/0926-860x(93)80232-F.

[76] M. Niwa, S. Sota, N. Katada, Strong Bronsted acid site in HZSM-5 created by mild steaming, Catal. Today, 185 (2012) 17-24, https://doi.org/10.1016/j.cattod.2011.09.028.

[77] Y. Miyamoto, N. Katada, M. Niwa, Acidity of beta zeolite with different Si/Al-2 ratio as measured by temperature programmed desorption of ammonia, Micropor. Mesopor. Mater., 40 (2000) 271-281, https://doi.org/10.1016/S1387-1811(00)00264-X.

[78] S. Suganuma, H.Y. Zhang, C.G. Yang, F.S. Xiao, N. Katada, Acidic property of BEA zeolite synthesized by seed-directed method, J. Por. Mater., 23 (2016) 415-421, https://doi.org/10.1007/s10934-015-0095-6.

[79] T. Armaroli, L.J. Simon, M. Digne, T. Montanari, M. Bevilacqua, V. Valtchev, J. Patarin, G. Busca, Effects of crystal size and Si/Al ratio on the surface properties of H-ZSM-5 zeolites, Appl. Catal. A: Gen., 306 (2006) 78-84, https://doi.org/10.1016/j.apcata.2006.03.030.

[80] J. Datka, B. Gil, A. Kubacka, Heterogeneity of OH groups in NaH-mordenites: Effect of Na/H exchange degree, Zeolites, 18 (1997) 245-249, https://doi.org/10.1016/S0144-2449(97)00009-2.

[81] A. Auroux, V. Bolis, P. Wierzchowski, P.C. Gravelle, J.C. Vedrine, Study of the Acidity of Zsm-5 Zeolite by Micro-Calorimetry and Infrared Spectroscopy, J. Chem. Soc. Faraday Trans. 1, 75 (1979) 2544-2555, https://doi.org/10.1039/f19797502544.

[82] F. Thibault-Starzyk, I. Stan, S. Abello, A. Bonilla, K. Thomas, C. Fernandez, J.P. Gilson, J. Perez-Ramirez, Quantification of enhanced acid site accessibility in hierarchical zeolites - The accessibility index, J. Catal., 264 (2009) 11-14, https://doi.org/10.1016/j.jcat.2009.03.006.

[83] T. Baba, N. Komatsu, Y. Ono, H. Sugisawa, Mobility of the acidic protons in H-ZSM-5 as studied by variable temperature H-1 MAS NMR, J. Phys. Chem. B, 102 (1998) 804-808, https://doi.org/10.1021/jp9720552.

[84] J. Kanellopoulos, C. Gottert, D. Schneider, B. Knorr, D. Prager, H. Ernst, D. Freude, NMR investigation of proton mobility in zeolites, J. Catal., 255 (2008) 68-78, https://doi.org/10.1016/j.jcat.2008.01.028.

[85] M.S. Katsiotis, M. Fardis, Y. Al Wahedi, S. Stephen, V. Tzitzios, N. Boukos, H.J. Kim, S.M. Alhassan, G. Papavassiliou, Water Coordination, Proton Mobility, and Lewis Acidity in HY Nanozeolites: A High-Temperature H-1 and Al-27 NMR Study, J. Phys. Chem. C, 119 (2015) 3428-3438, https://doi.org/10.1021/jp513030w.

[86] R. Osuga, T. Yokoi, K. Doitomi, H. Hirao, J.N. Kondo, Infrared Investigation of Dynamic Behavior of Bronsted Acid Sites on Zeolites at High Temperatures, J. Phys. Chem. C, 121 (2017) 25411-25420, https://doi.org/10.1021/acs.jpcc.7b09846.

[87] P. Losch, H.R. Joshi, O. Vozniuk, A. Grunert, C. Ochoa-Hernandez, H. Jabraoui, M. Badawi, W. Schmidt, Proton Mobility, Intrinsic Acid Strength, and Acid Site Location in Zeolites Revealed by Varying Temperature Infrared Spectroscopy and Density Functional Theory Studies, J. Am. Chem. Soc., 140 (2018) 17790-17799, https://doi.org/10.1021/jacs.8b11588.

Table 1: Dealumination conditions and aluminum concentration in YNU-5 samples

Sample	Nitric acid treatment			Si/Al molar ratio	[Al] / mol kg^{-1}
	[HNO_3] / mol dm^{-3}	Heating method	Time / h		
H-YNU-5				10.7	1.44
stable deAl-YNU-5	2	refluxed in 403 K-oil bath	24	50.7	0.323
unstable deAl-YNU-5	3	heated at 353 K in oil bath	2	49.8	0.329
Deeply-deAl-YNU-5	13.4	refluxed in 403 K-oil bath	24	294	0.056

Table 2: Enthalpy of ammonia desorption and energies of framework **YFI** models estimated by quantum calculations

Position*	Multiplicity	Direction of acidic H	Enthalpy of ammonia desorption (ΔH) / kJ mol^{-1}	Relative energy of $Zeo[(SiO_2)_{119}(AlO_2)_1]^-$ / kJ mol^{-1} **	Energy of dealumination [reaction (1)] / kJ mol^{-1}
Al1O7Si3	16	Isolated 8-ring	164.35	0	-18
Al1O20Si1	8	Isolated 8-ring	150.65		
Al1O21Si5	8	Isolated 8-ring	157.76		
Al2O1Si9	16	Connected 8-ring	143.04	2	-65
Al2O4Si2	32	Connected 8-ring	141.72		
Al2O13Si8	16	12-ring	128.66		
Al3O7Si1	16	Isolated 8-ring	137.17	22	-45
Al3O16Si4	16	Connected 8-ring	139.50		
Al3O17Si6	16	12-ring	124.65		
Al3O18Si9	16	Connected 8-ring	141.45		
Al4O3Si4	8	12-ring	101.22	0	-2
Al4O9Si4	8	Connected 8-ring	161.08		
Al4O16Si3	8	Connected 8-ring	100.92		
Al5O19Si8	16	Isolated 8-ring	-339.67	7	8
Al5O21Si1	8	Isolated 8-ring	160.91		
Al5O22Si5	8	Isolated 8-ring	165.25		
Al6O10Si6	16	Isolated 8-ring	152.35	2	-57
Al6O12Si6	16	12-ring	123.95		
Al6O14Si7	16	Isolated 8-ring	148.00		
Al6O17Si3	16	12-ring	127.60		
Al7O2Si7	16	Isolated 8-ring	148.90	34	-56
Al7O6Si8	16	12-ring	127.08		
Al7O11Si7	16	12-ring	119.07		
Al7O14Si6	16	Isolated 8-ring	149.96		
Al8O6Si7	16	12-ring	131.17	35	-49
Al8O8Si9	16	12-ring	123.34		
Al8O13Si2	16	12-ring	130.72		
Al8O19Si5	16	Isolated 8-ring	130.56		
Al9O1Si2	16	12-ring	127.27	36	-67
Al9O8Si8	16	12-ring	127.32		
Al9O15Si9	16	12-ring	168.50		
Al9O18Si3	16	12-ring	123.99		

*: Al*i*O*j*Si*k* shows that the Al and Si atoms are located at T*i* and T*k* sites, whereas the proton is bonded to oxygen atom at O*j* site. The numbering of sites is according to the original report on YNU-5.[37]

**: Difference between the total energy of discussed model and the minimum value among the sites shown here.

Figure captions

Figure 1: Schematic illustration of 12-ring system and isolated 8-ring channel in **YFI** framework viewed along *c*-axis.

Figure 2: Plots of Brønsted (●, ◆, ■, ▲, ▼, ●, ▼, ● and ▼) and Lewis (○, ◇, □, △, ▽, ○, ▽, ○ and ▽) acid amounts measured by ammonia IRMS-TPD (●, ◆, ■, ▲, ▼, ○, ◇, □, △ and ▽), IR of adsorbed pyridine (●, ▼, ○ and ▽) and IR of CD_3CN (●, ▼, ○ and ▽) on H-YNU-5 (●, ●, ●, ○, ○, and ○), HNaK-YNU-5 with different [Na] and [K] (◆ and ◇), stable deAl-YNU-5 (■ and □), unstable deAl-YNU-5 (▲ and △) and deeply-deAl-YNU-5 (▼, ▼, ▼, ▽, ▽ and ▽).

Figure 3: Distribution of ammonia desorption enthalpy of Brønsted acid sites on zeolites with various structures, where C_w shows the concentration of Brønsted acid sites per unit weight of zeolite, and ΔH shows the standard molar enthalpy of ammonia desorption.

Figure 4: 3500−3800 cm^{-1} region of IR spectrum of (A) evacuated *in situ* H-YNU-5 zeolite, followed by (B) exposure to pyridine vapor and (C) further treatment with ammonia at 343 K.

Figure 5: 1300−1800 cm^{-1} region of IR spectra of *in situ* H-YNU-5 zeolite after (b) exposure to pyridine vapor, (c0) further treatment with ammonia at 343 K and elevation of temperature (c1: 373 K, c2: 473 K, c3: 573 K, c4: 673 K, c5: 773 K), shown by difference [spectrum after exposure - spectrum before exposure (A)].

Figure 6: 3500−3800 cm^{-1} region of IR spectra of (A) evacuated stable deAl-YNU-5 zeolite, followed by (B) exposure to pyridine vapor and (C) further treatment with ammonia at 343 K.

Figure 7: 1200−1800 cm^{-1} region of IR spectra of stable deAl-YNU-5 zeolite after (b) exposure to pyridine vapor, (c0) further treatment with ammonia at 343 K and elevation of temperature (c1: 373 K, c2: 473 K, c3: 573 K, c4: 673 K, c5: 773 K), shown by difference [spectrum after exposure - spectrum before exposure (A)].

Figure 8: 3500−3800 cm^{-1} region of IR spectra of (A) evacuated unstable deAl-YNU-5 zeolite, followed by (B) exposure to pyridine vapor and (C) further treatment with ammonia at 343 K.

Figure 9: 1200−1800 cm^{-1} region of IR spectra of unstable deAl-YNU-5 zeolite after (b) exposure to pyridine vapor, (c0) further treatment with ammonia at 343 K and elevation of temperature (c1: 373 K, c2: 473 K, c3: 573 K, c4: 673 K, c5: 773 K), shown by difference [spectrum after exposure - spectrum before exposure (A)].

Figure 10: Positions of protons calculated to show (red) >140 or (blue) <140 kJ mol^{-1} of ammonia desorption enthalpy viewed from *c*-axis directions of **YFI** structure.

Figure 11: Calculated distribution of ammonia desorption enthalpy of Brønsted acid sites in 8- and 12-rings of **YFI** structure. The number of acid site models with ΔH in every 5 kJ mol^{-1} region is counted from Table 2, and the sum of multiplicity is plotted against ΔH.

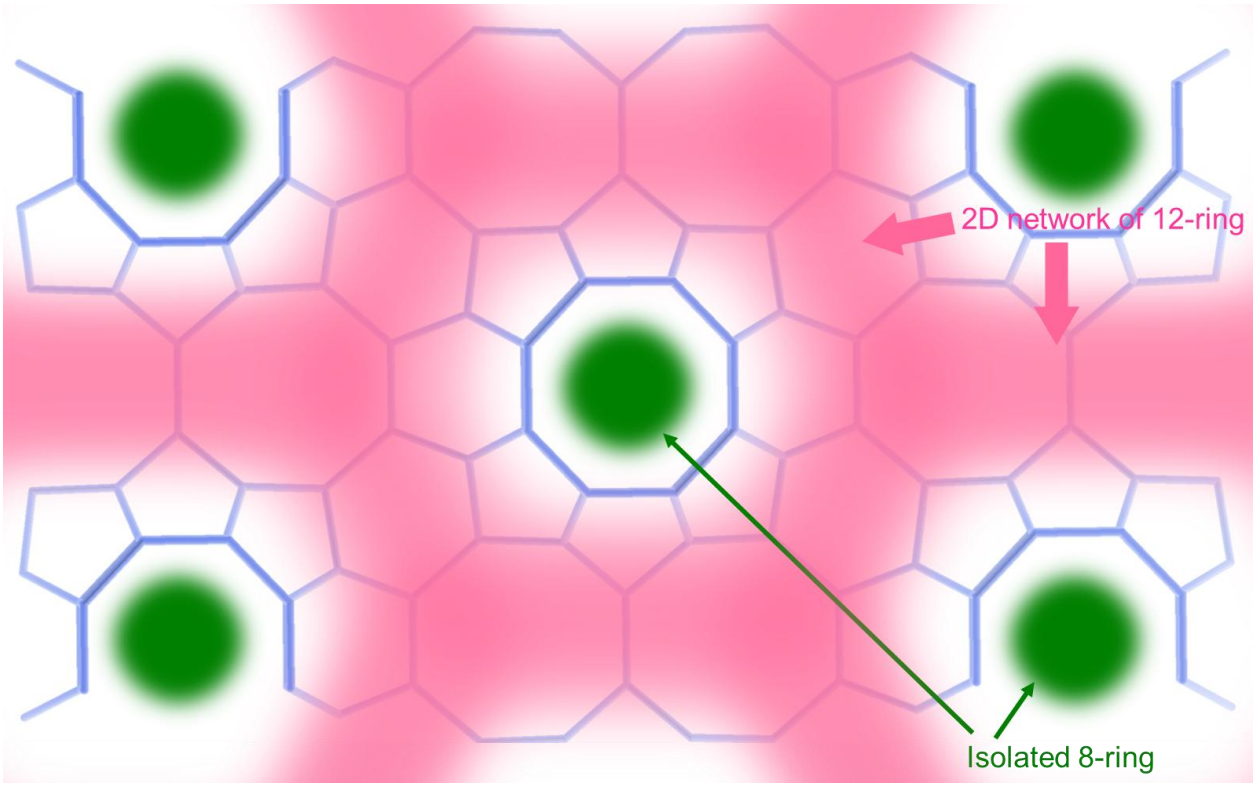

Figure 1

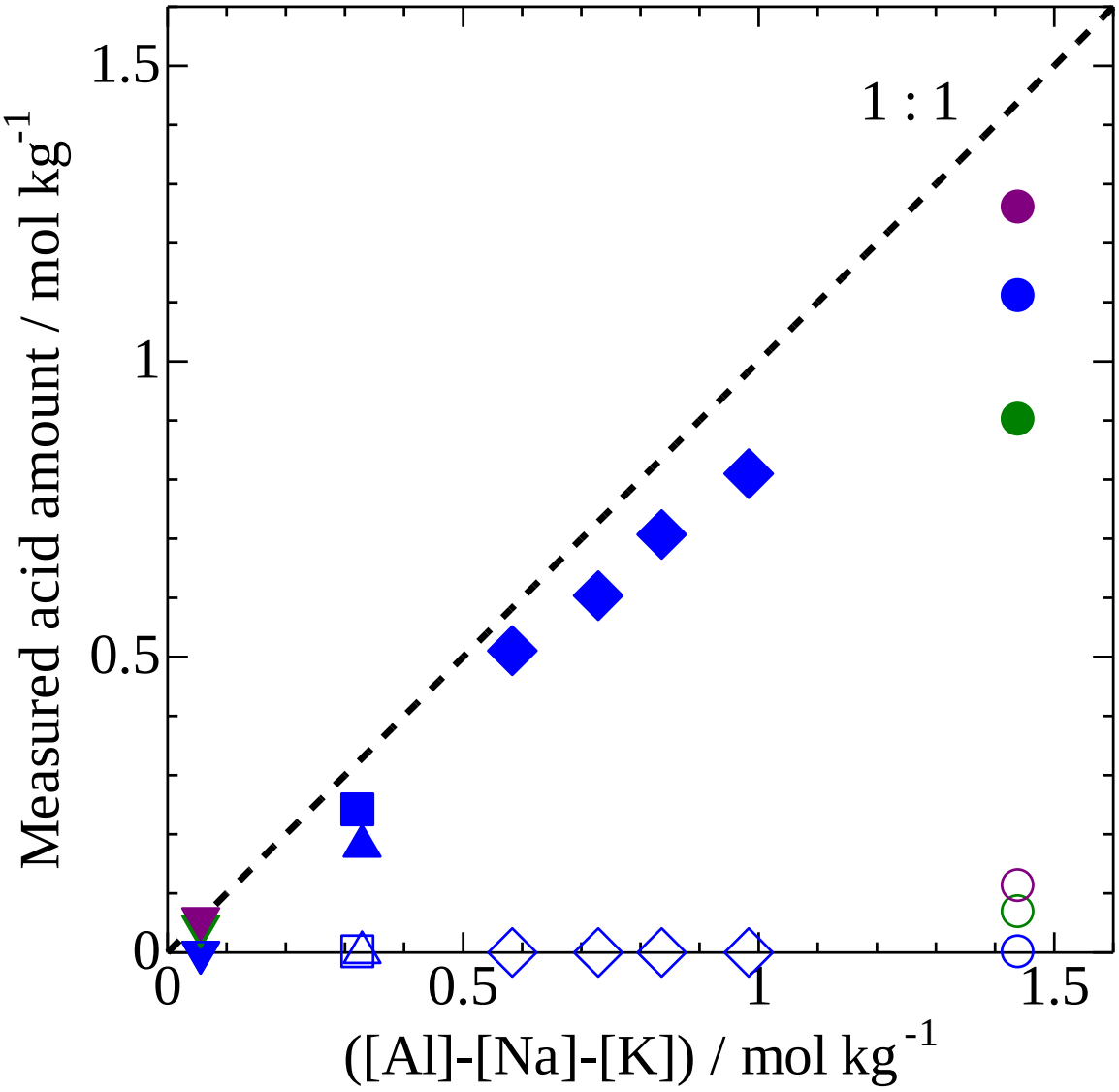

Figure 2

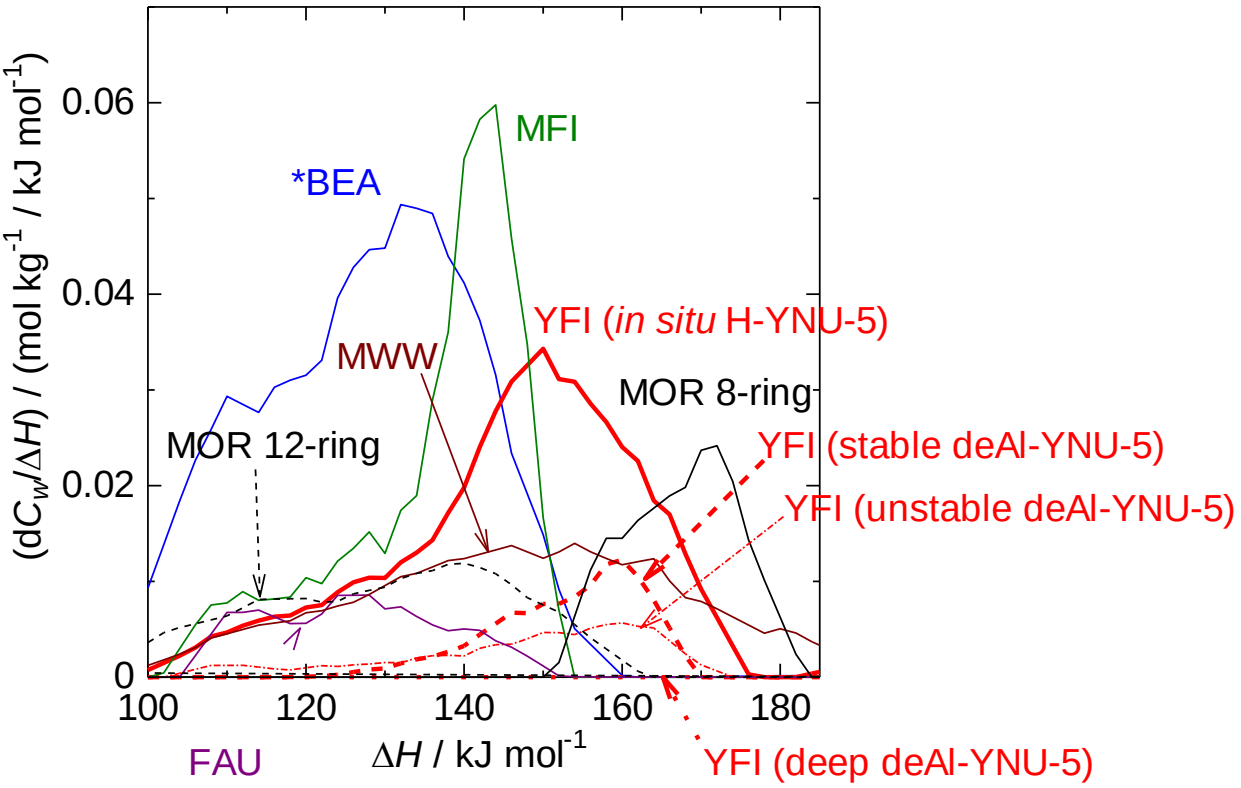
0.06
0.04
0.02
0
100
120
140
160
180
$(dC_w/\Delta H)$ / (mol kg^{-1} / kJ mol^{-1})
ΔH / kJ mol^{-1}
*BEA
MFI
MWW
MOR 12-ring
MOR 8-ring
YFI (*in situ* H-YNU-5)
YFI (stable deAl-YNU-5)
YFI (unstable deAl-YNU-5)
YFI (deep deAl-YNU-5)
FAU

Figure 3

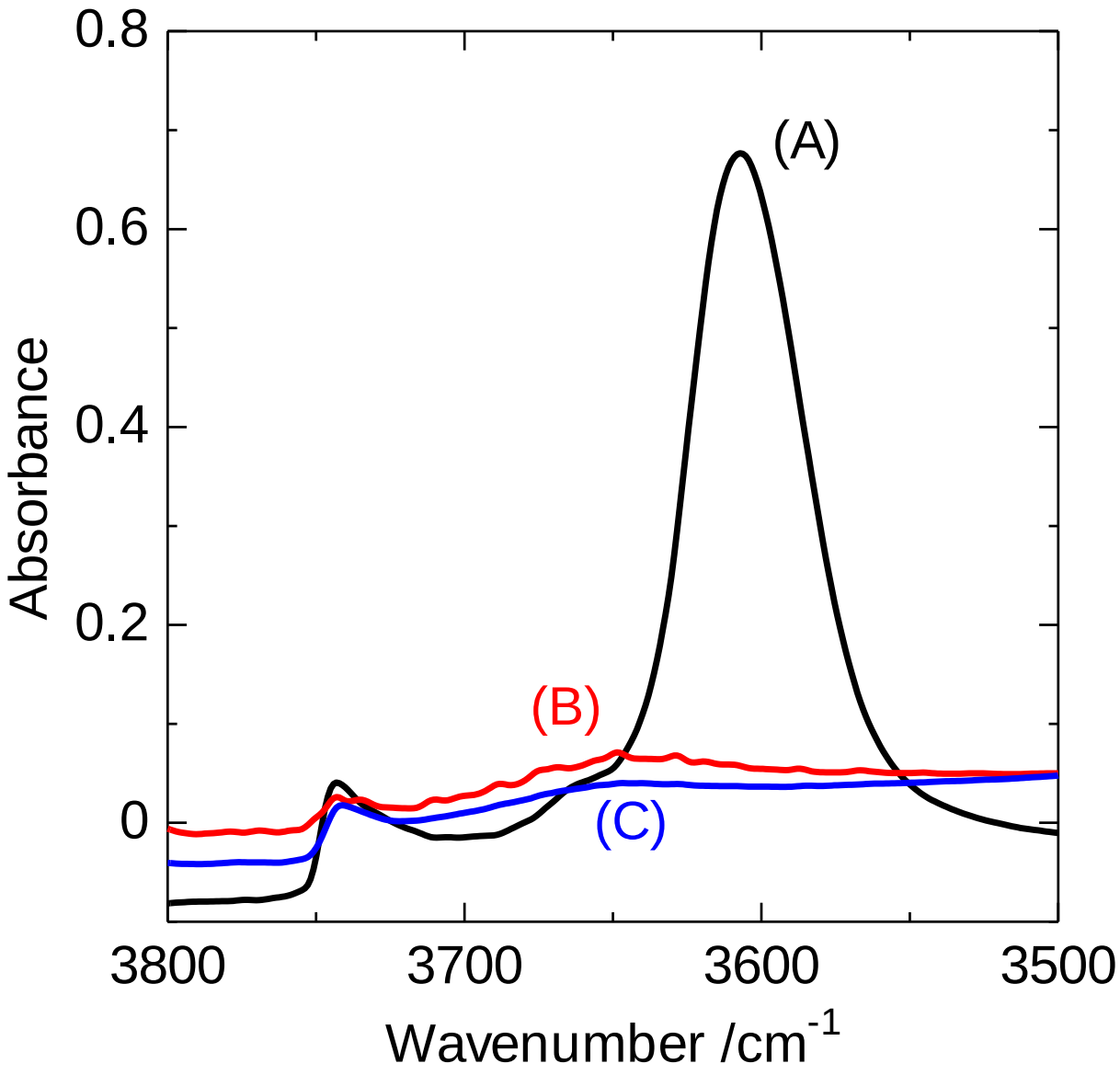
0.8
0.6
0.4
0.2
0
Absorbance
(A)
(B)
(C)
3800
3700
3600
3500
Wavenumber /cm-1

Figure 4

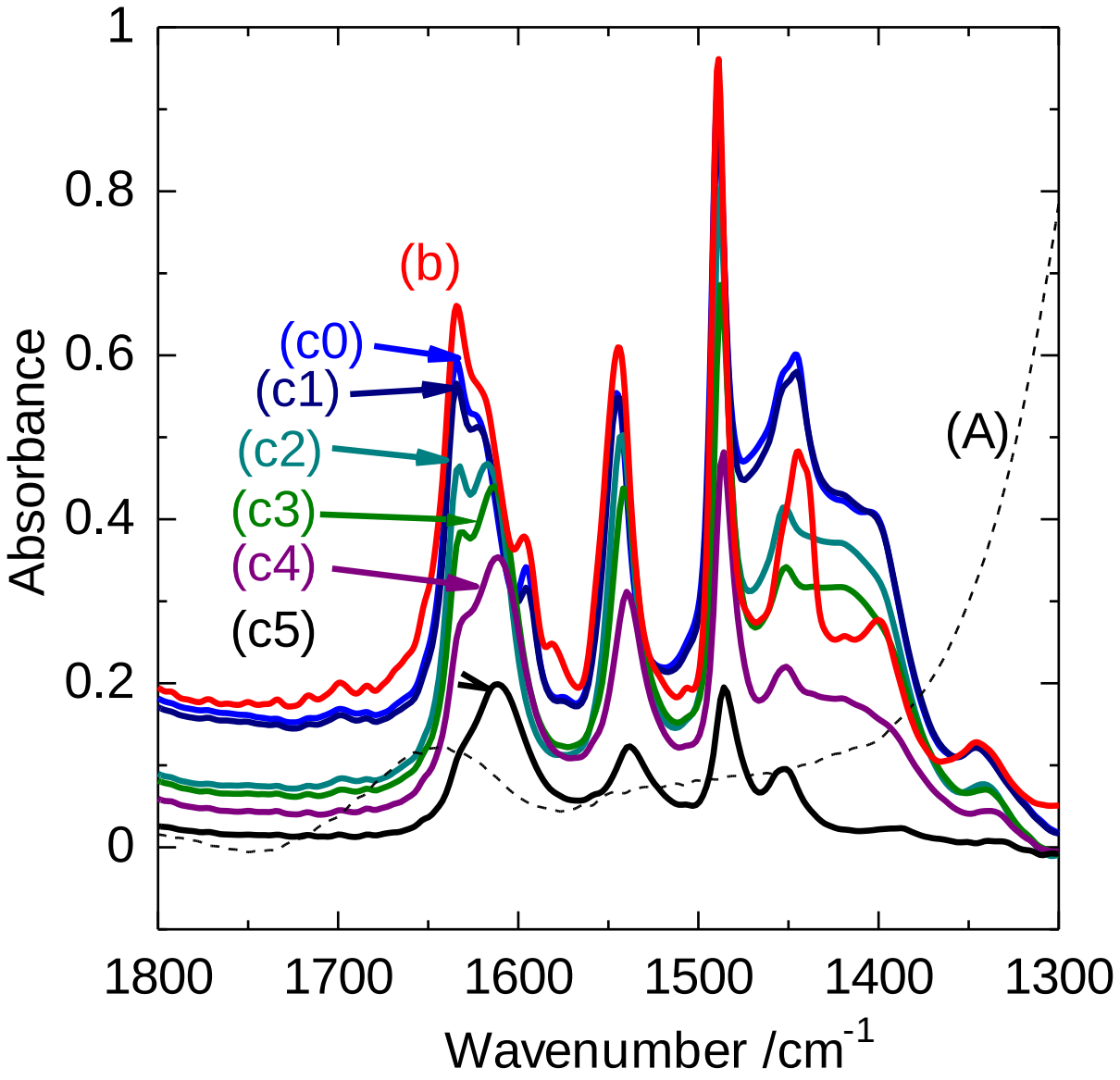
1
0.8
0.6
0.4
0.2
0
Absorbance
(b)
(c0)
(c1)
(c2)
(c3)
(c4)
(c5)
(A)
1800
1700
1600
1500
1400
1300
Wavenumber /cm-1

Figure 5

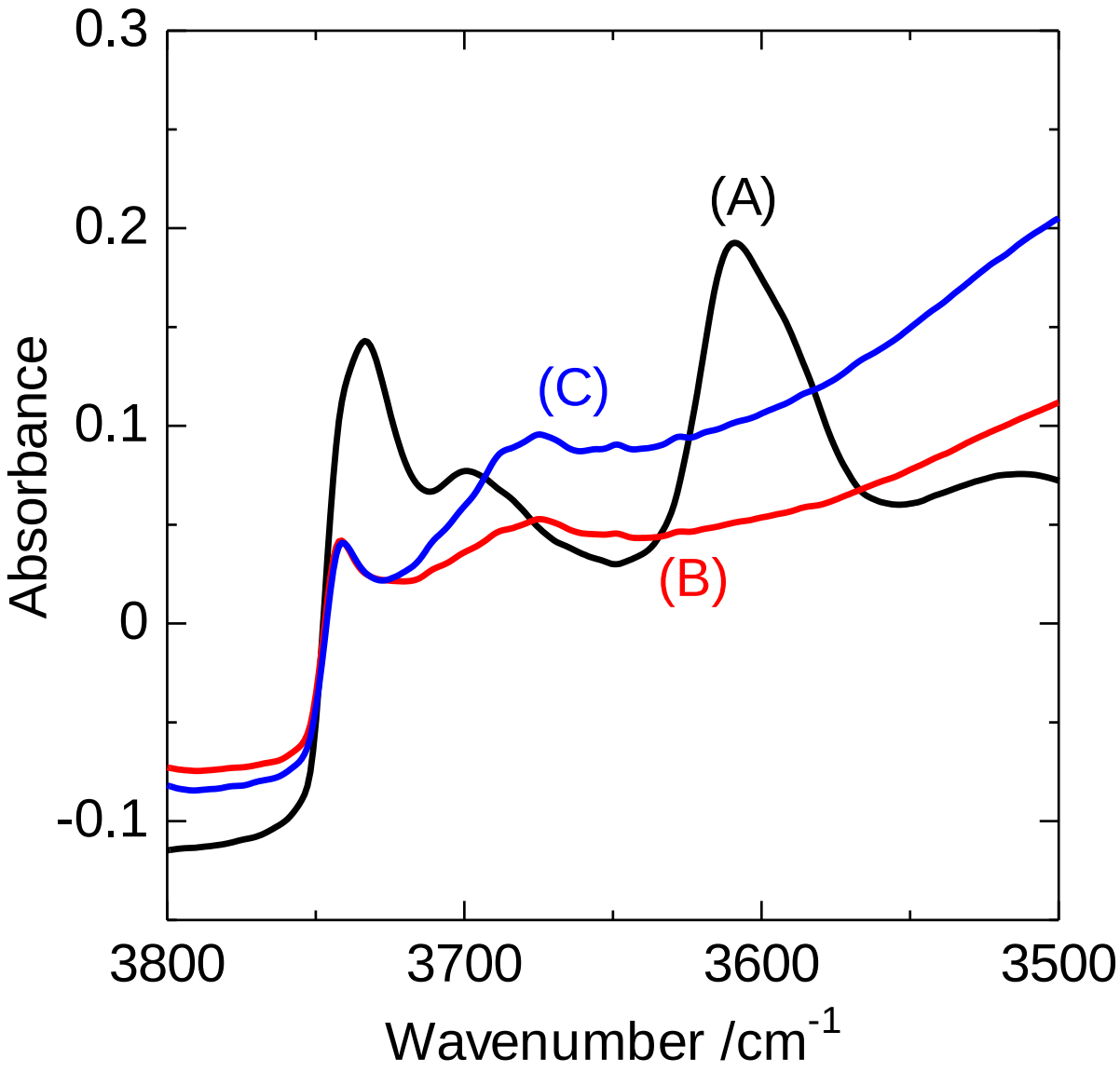
0.3
0.2
0.1
0
-0.1
Absorbance
(A)
(C)
(B)
3800
3700
3600
3500
Wavenumber /cm-1

Figure 6

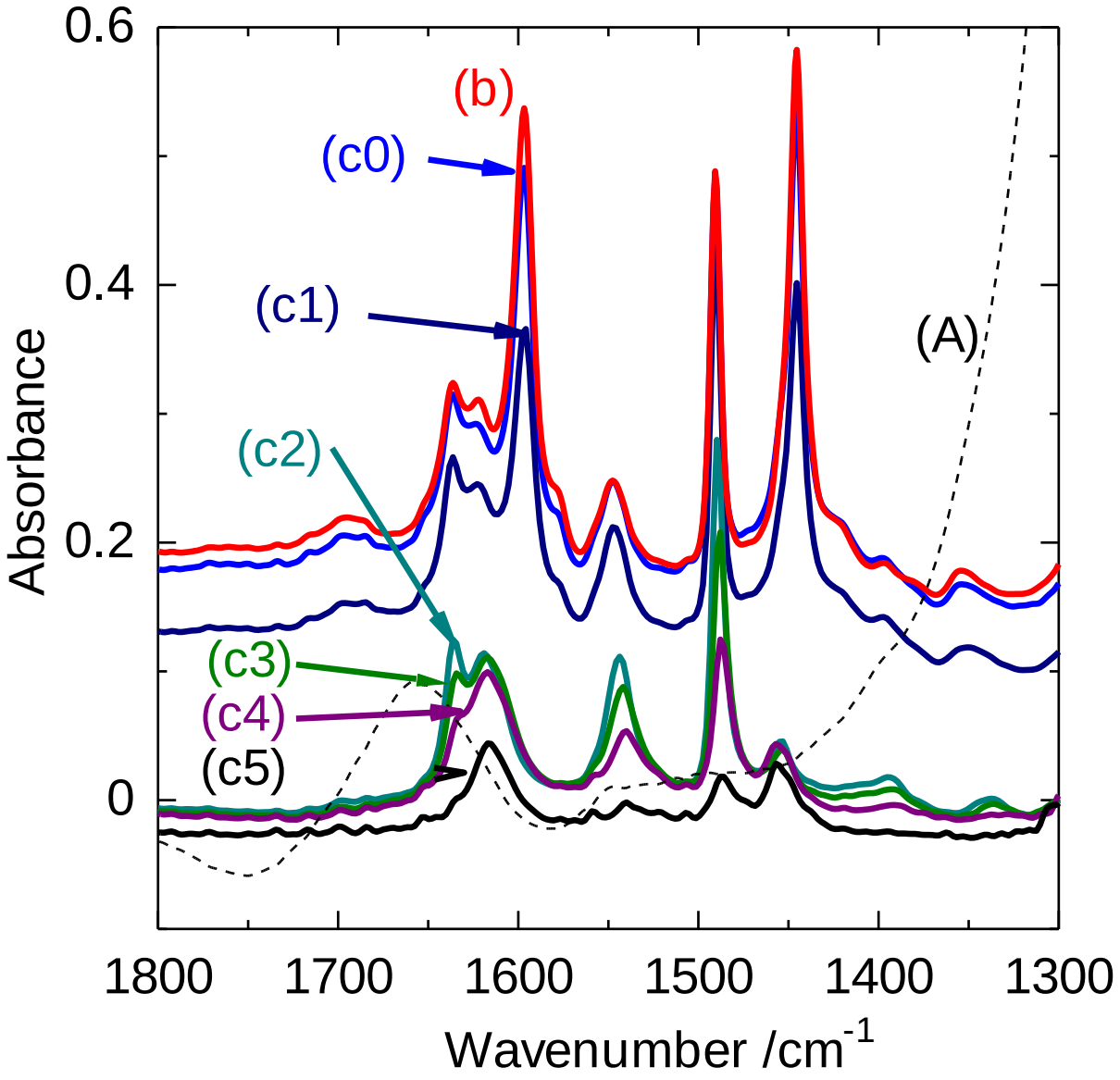
0.6
0.4
0.2
0
Absorbance
(b)
(c0)
(c1)
(c2)
(c3)
(c4)
(c5)
(A)
1800
1700
1600
1500
1400
1300
Wavenumber /cm-1

Figure 7

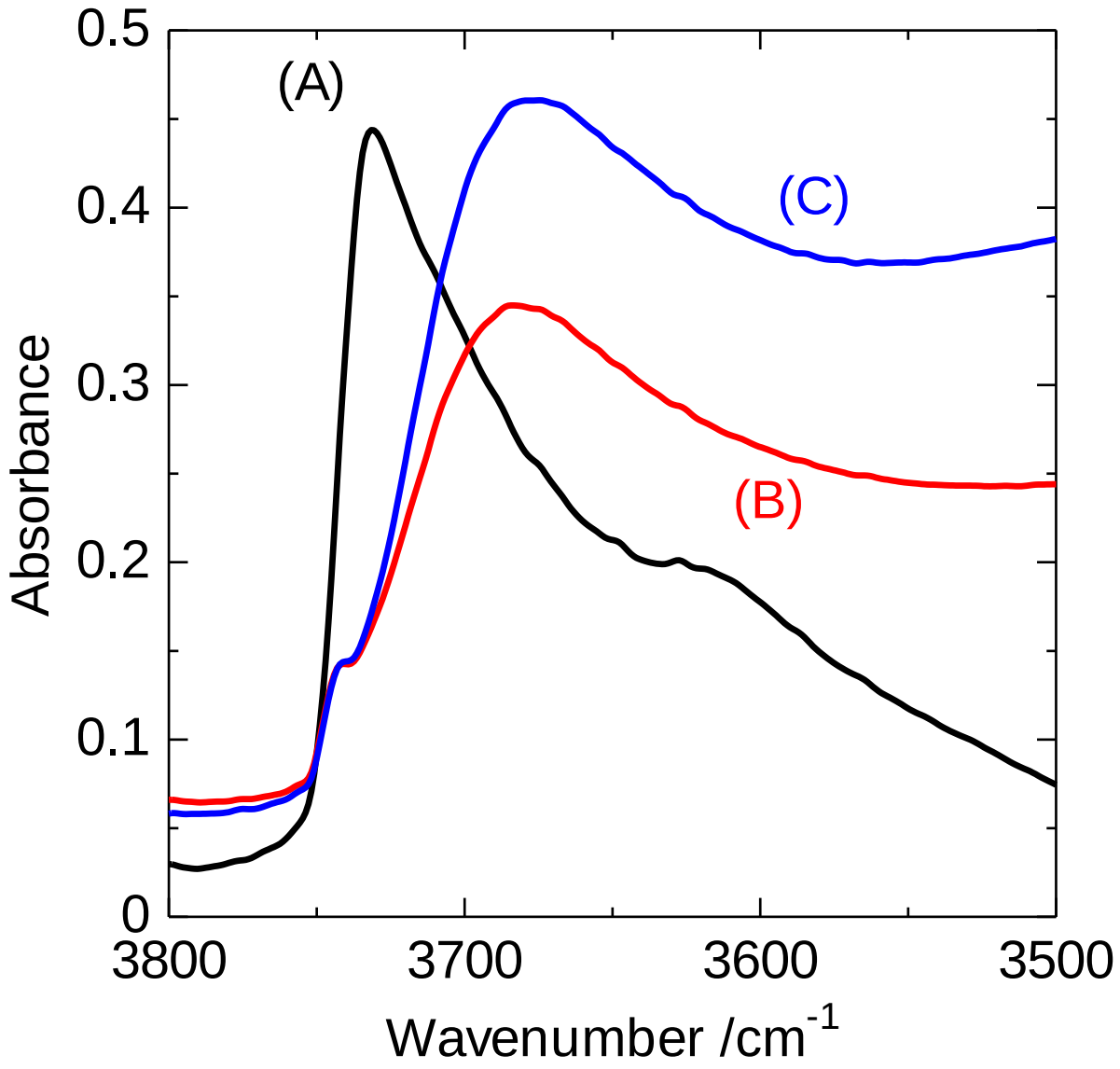
0.5
0.4
0.3
0.2
0.1
0
Absorbance
(A)
(C)
(B)
3800
3700
3600
3500
Wavenumber /cm-1

Figure 8

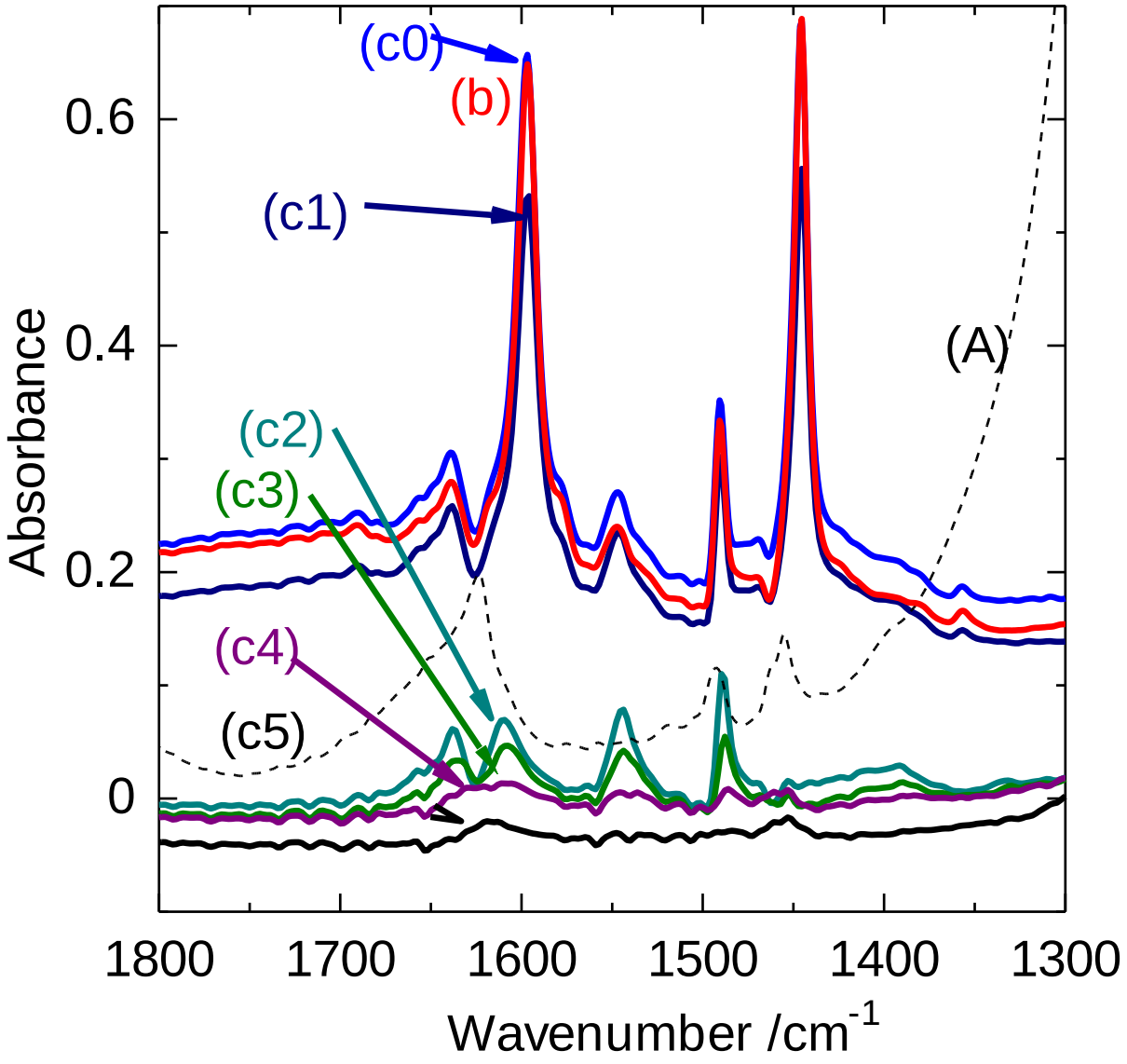
(c0)
(b)
(c1)
(A)
(c2)
(c3)
(c4)
(c5)
Absorbance
0.6
0.4
0.2
0
1800
1700
1600
1500
1400
1300
Wavenumber /cm-1

Figure 9

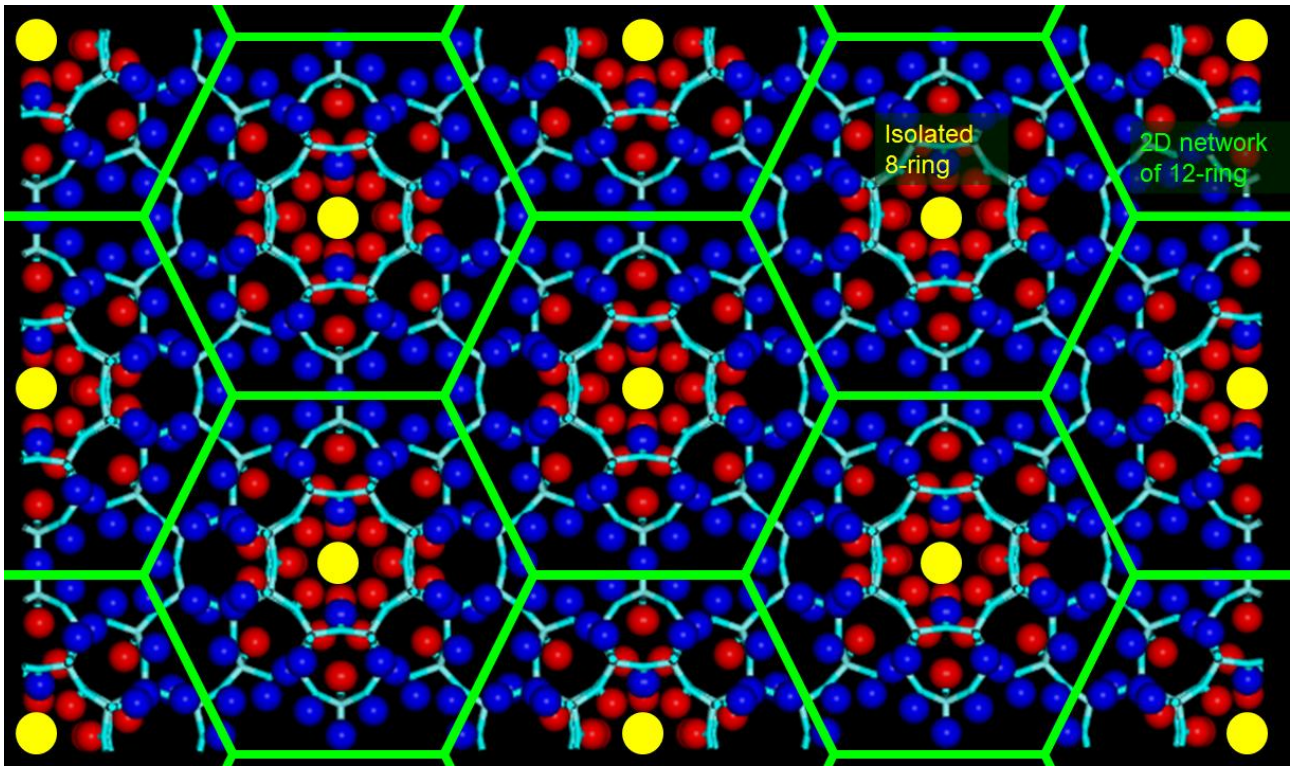

Figure 10

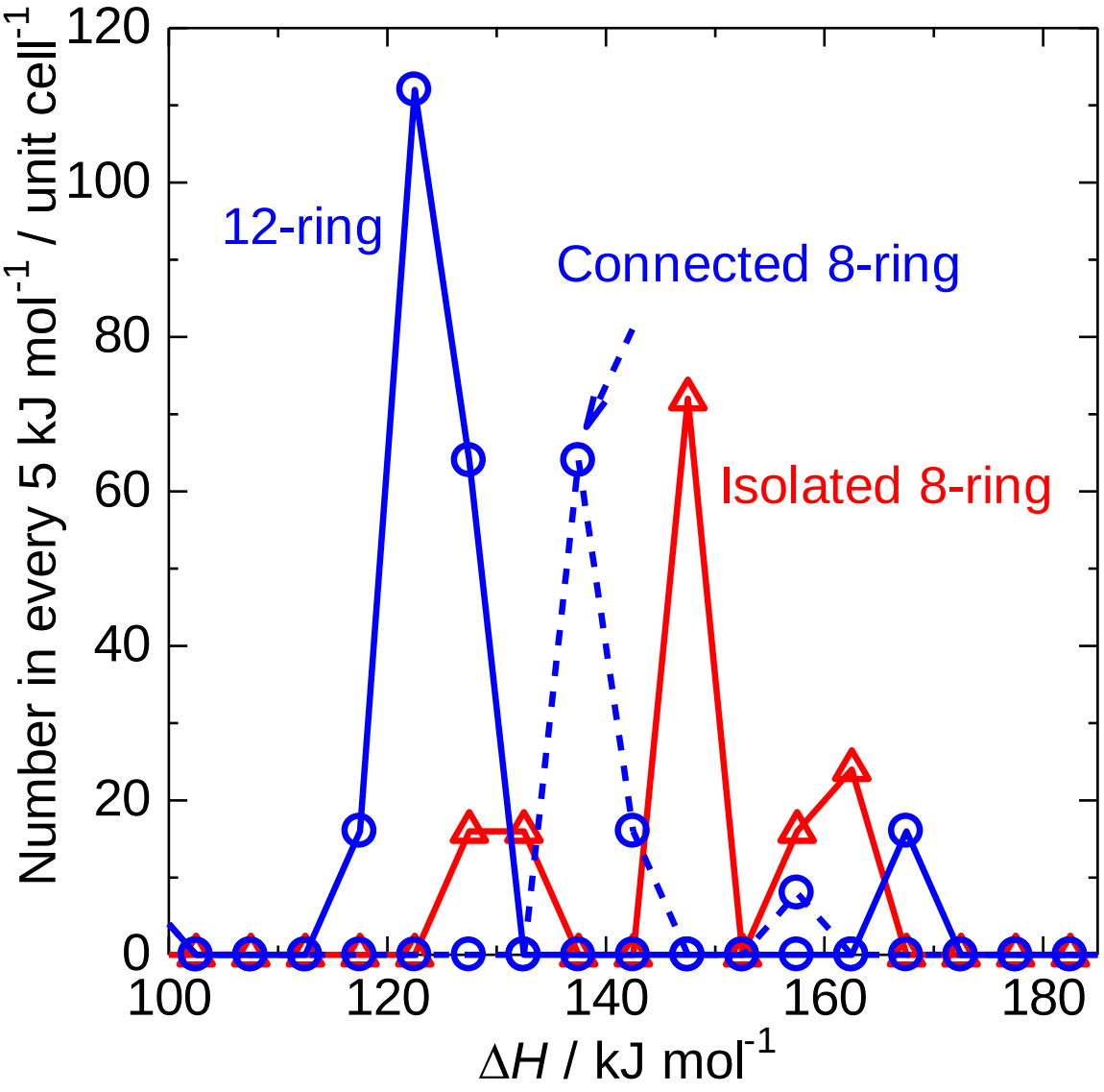
12-ring
Connected 8-ring
Isolated 8-ring
Number in every 5 kJ mol-1 / unit cell-1
ΔH / kJ mol-1
0
20
40
60
80
100
120
100
120
140
160
180

Figure 11